

Mechanical and histological characterization of
thrombi retrieved during thrombectomy for acute
ischaemic stroke

by

Philip Snouckaert van Schauburg

to obtain the degree of

Master of science
in Biomedical Engineering

at the Delft University of Technology,
to be presented on the Tuesday December 12, 2019 at 13:45

Student number: S2410451

Supervisors: Prof. dr. Frans van der Helm & Dr.ir. Frank Gijzen

Contents

Preface	v
Acknowledgements	vii
1 Scientific paper	1
Introduction	2
Methods	3
Results	4
Discussion	6
Conclusion	9
A Mechanical force tester	11
A.1 Materials and setup	11
A.2 Software	13
A.3 Validation	13
B Collection, preparation and testing of thrombus samples	17
B.1 Thrombus collection and preparation	17
B.2 Unconfined compression test	19
B.2.1 Compression profile	19
B.2.2 Data analysis	20
B.2.3 Results	21
C Histology	23
C.1 Methods	23
C.2 Results	25
D Constitutive modelling	29
D.1 Application of the Mooney-Rivlin model to experimental data	29
D.2 Derivation of the stress equation for a Mooney-Rivlin fit	30
D.3 Matlab code for calculation of secant and tangent moduli	33
D.4 Results	35
E Micro indentation	37
E.1 Methods	37
E.2 Results	40
F Protocols	45
Collection, preparation and unconfined compression	46
Tissue embedding	56

Preface

Acute ischaemic stroke (AIS) is a condition where a blood clot acutely blocks a cerebral artery which results in the sudden loss of blood flow towards the brain. The acute obstruction, the rapid deterioration of the inflicted brain tissue and the limited treatment possibilities have made AIS reach the top 5 causes of death world wide. As a biomedical engineering student, I aim to work in an environment which strongly contributes to the improvement of patient outcome, especially of those effected by such detrimental diseases. I was provided with the opportunity to contribute to the improvement of stroke treatment by fulfilling a part of the *In Silico Clinical Trials for treatment of Acute ischaemic stroke* (INSIST) project, for which I am grateful.

This thesis is the final result of my master in Biomedical engineering at the TU Delft and of my graduation research project at the Erasmus Medical Center Rotterdam. The aim of this project was to determine the relation between the biomechanical properties and the composition of fresh thrombi retrieved from AIS patients. In aim of fulfilling this goal, I have gained a valuable experience due to diversity of challenges which were to overcome and the people with whom I have gotten to work, covering all aspects of what I believe the field of biomedical engineering has to offer. Firstly, setting up a collaboration with the radiology department to collect fresh thrombi has allowed me to experience the clinical practices of a thrombectomy procedure first hand many times. Secondly, creating a custom made force tester, performing experiments on a micro- and macro-scale and analysing the acquired data provided the challenge of solving technical issues. Lastly, relating the mechanical to biological aspects, by performing histological analysis, additionally provided the necessary experience in the biological field, of which I have noticed that the knowledge is fundamental in solving biomedical issues.

The result of my work is written in a the brief form of a Scientific paper. As the paper is aimed towards readers in the clinical field, multiple key aspects of the research have not been described in full detail or have been left out completely. Therefore, additional information has been provided in the appendices.

I have enjoyed all the work that has lead to this final thesis and I hope you enjoy reading it just as much.

*Philip Snouckaert van Schauburg
Delft, December 2019*

Acknowledgements

This project had not have succeeded without the help of a number of people. Firstly, I would like to thank Aad van der Lugt for providing me with the opportunity to take on this project. Our brief yet enthusiastic meetings have always been of great motivation and have driven me to achieve the best result possible.

Many thanks go out to Heleen van Beusekom for her help and guidance throughout the entire project with regards to histological matters, laboratory practices and unplanned chats. Additionally, Kim van Gaalen has aided with the histological analysis and provided assistance by sectioning and staining samples at a crucial point during this project, for which I am thankful.

I would like to thank Michiel Manten for machining the required parts for the force tester and for thinking along with the designing of all other created tools. Robert Beurskens for all the time we spent connecting all the hardware and setting up the force tester. Bram van der Eerden for providing me with access to his lab, the Piuma nano-indenter and all necessary facilities.

Also I wish to thank prof. Frans van der Helm for supervising me during the course of this project. I greatly valued his opinion and the feedback he provided along the way in order to improve the result of the research.

Lastly, I would like to express my sincere gratitude to Nikki Boodt and Frank Gijsen, as they have provided me with excellent supervision, a great resource of both clinical and engineering knowledge and support throughout the entire project.

1

Scientific paper

Mechanical and histological characterization of thrombi retrieved during thrombectomy for acute ischaemic stroke

Philip Snouckaert, 4507479

Technical University of Delft - Erasmus Medical Center Rotterdam

Background: The efficacy of a thrombectomy procedure for acute ischaemic stroke (AIS) is largely dependent on mechanical behaviour of thrombi and interactions with the thrombectomy device. Studies have examined clot analogues and evidence suggests that thrombus mechanical properties largely depend on composition, yet evidence based on thrombi retrieved from AIS patients is still lacking. Therefore, this study aims to characterize the mechanical properties of thrombi retrieved from AIS patients and to determine the relation to thrombus composition. Additionally, results were compared to literature in order to assess clot analogue representativeness.

Methods: Directly following a thrombectomy procedure, unconfined compression tests were performed on thrombi retrieved from acute ischaemic stroke patients. For all tested samples, the material properties were characterized and related to the histologically determined composition. Identified histological components were 1) Fibrin & platelets, 2) Red blood cell and 3) Leukocytes. A subgroup analysis was performed to compare values with literature, where samples were stratified into four groups based on fibrin & platelet content (F&P -low, -moderate low, -moderate high and -high).

Results: A total of 18 patients yielded 39 samples which were successfully tested and histologically analysed. Sample stiffness was found to be positively correlated to fibrin & platelet content ($R_s=0.69$, $p<0.001$). A good histological distribution was present within the data, as the fibrin & platelet content ranged from 7% to 99%. Subgroup analysis showed little difference in mechanical behaviour between the F&P moderate-low and F&P moderate-high subgroups, with the F&P low and F&P high groups respectively exhibiting a decreased and increased stiffness. Comparing to current literature, the results demonstrated that analogues most accurately resemble thrombi with a low fibrin & platelet content. Furthermore, all samples displayed viscoelastic and non-linear stress-strain behaviour.

Conclusion: It was found that composition is a strong influencing factor of thrombus mechanical properties. Both at high and low fibrin & platelet contents, the relation between composition and stiffness was strongest, while it was least pronounced at moderate fibrin & platelet contents (approximately 25%-75%).

I. Introduction

Mechanical thrombectomy has recently become the standard of care for treatment of acute ischaemic stroke (AIS) patients, where recanalization of the obstructed intracranial vessel is achieved with use of a stent retriever or aspiration device. These procedures dependent on the interactions between the thrombus and the device, where the mechanical properties of thrombi will be of influence on retrieval success. It has been shown that thrombus material retrieved from AIS patients mainly consist of fibrin fibres, erythrocytes, leukocytes and platelets and that the composition can vary greatly between thrombi.^{1,2} Although it can be expected that thrombus mechanical behaviour is dependent on composition, currently only one study has analysed the mechanical properties of thrombi retrieved from AIS patients. *Chueh et al.* assessed thrombi retrieved from AIS patients by subjecting the samples to compressive loads.³ However, the examined thrombi were retrieved from 4 AIS patients, histologically very similar and uniform in mechanical behaviour. As it has now become evident that thrombi can fluctuate significantly in composition,^{1,2} additional research is required to determine the mechanical

behaviour of a wider range of thrombi with varying compositions. Multiple studies have assessed thrombus analogues under various loading conditions, providing evidence that fibrin is the main contributor to thrombus stiffness.^{4,5,6,7} However, as analogues are made *in vitro*, the environment in which they originate can differ significantly between studies and frequently does not resemble physiological conditions. As very limited research has been performed on the mechanical characterization of thrombi retrieved from AIS patients, it is uncertain how composition effects thrombus mechanical behaviour and whether the mechanical properties of analogues are representative for those originated *in vivo*. Therefore, the goal of this study is to define the relation between the mechanical properties and composition of thrombi retrieved from AIS patients. Additionally, findings are compared with literature to assess the representativeness of analogues.

II. Methods

Patient inclusion

Thrombus material was retrieved from patients that underwent endovascular treatment for AIS from July to

October 2019 in The Erasmus Medical Center in Rotterdam. Patients that met the following criteria were included in the present study: age 18 years and older, a proximal intracranial vessel occlusion in the anterior or posterior circulation, as shown on computed tomography angiography, and successful retrieval of thrombus material. Deferred informed consent was obtained for all patients following the thrombectomy procedure.

Collection and preparation of thrombus samples

Retrieved thrombus material was preserved in Dulbeccos modified Eagles medium (DMEM, high glucose, L-glutamine, HEPES, no phenol red. Thermo Fischer, Waltham, MA) and kept at 4-10 °C during transportation and short-term storage as it creates a non-destructive environment which adequately preserves cell structures and tissue mechanical properties. Thrombus material was collected and mechanically tested immediately after retrieval. The material was collected and tested within a maximum period of 12 hours following the procedure. An in-house developed trimming fixture was used to cut 1mm samples from the thrombus material, such that they consisted of a flat top and bottom surface. Thrombus material was photographed at multiple stages, before and after trimming, together with a ruler to provide a dimensional reference. Additional details regarding the preparation of samples can be found in appendix B.

Mechanical characterization

Mechanical properties of samples were determined by means of an unconfined compression experiment, as it is a well standardized method suitable for the evaluation soft biological tissue. The technique is reported in literature for the assessment of clot analogues and is currently the only method used for the mechanical analysis of material retrieved from AIS patients. Thrombi are subjected to compressive loads at multiple stages during the processes of occlusion and recanalization of an intracranial artery, therefore making this technique suitable to partly replicate the forces and interactions subjected to a thrombus *in vivo*.

The experiments were performed with use of a custom-built force tester, consisting of an aluminium compression plate, attached to a 2,5N load cell (LSB200 Jr. Miniature S-beam load cell, Futek), which was vertically driven by a linear actuator (EACM4-E15-AZMK, Oriental motor). Technical specifications and details on equipment validation can be found in appendix A. All experiments were performed with samples submerged in DMEM at 37±1 °C to replicate physiological conditions. Pre-conditioning, loading of a sample with relatively small strains, is often performed before the start of an experiment to increase the reproducibility of the results. However, during a thrombectomy procedure, a thrombus is immediately subjected to the full compressive load exerted by the stent. This is accounted for by performing the experiment without preconditioning of sample.

Samples were subjected to 80% compression, at a strain rate of 10%/s, after which retraction was immediately initiated and executed at an identical rate. The applied strain allows for the assessment of the mechanical behaviour at both small and large deformations, in accordance with literature. Regardless of permanent damage occurring within the sample as a result of the applied strain, limiting deformation to 80% allows for repetitive loading of the sample. The compression cycle was repeated 20 times to assess the materials response to repetitive loading. Nominal stress and nominal strain values were used to assess the samples stress-strain response. Due to the irregular and non-circular shape of the samples, the acquired photographs were used to determine the cross-sectional areas in ImageJ software (1.52a, National Institutes of Health, USA), using the ruler as a reference for determining the pixel to unit length ratio. Additional information regarding the experimental protocol can be found in appendix B and E.

Data analysis and constitutive modelling

An unconfined compression test provides data to assess thrombus behaviour, which is represented in a graph, showing the measured stress which corresponds to the applied deformation (a stress-strain curve). To obtain the mechanical properties of the tested material, first the raw biomechanical data, derived from the unconfined compression experiments, was mathematically described using constitutive models. The resulting equations allow for the derivation of material properties and additionally provide the means for further modelling applications. A first order Mooney-Rivlin model was chosen to describe the experimental test data yielded from the unconfined compression test. Fitting of the models to the experimental data was performed in Abaqus (2016, Dassault Systems, Johnston, RI).

To address the (non-linear) mechanical behaviour of the tested samples, the stiffness was calculated at multiple strains. As a measure for the stiffness, the tangent modulus was determined, which is defined as the slope of a line which is tangent to any point of interest on the curve, as is exemplified in figure 2. It is denoted as tangent E_x , where x is the percentage deformation corresponding to the reported stiffness. Details regarding constitutive modelling and derivation of material properties can be found in appendix used and the results obtained can be found in appendix D.

Histopathological analysis

Following the compression test, samples were fixated in formaldehyde, embedded in paraffin wax and sectioned in 5µm thick sections at a depth of 200µm. The orientation of the sample was tracked throughout the process in order to embed the sample such that the initial section was cut along the samples top surface. Sections were stained with hematoxylin and eosin (H&E). Samples were scanned and visualized at 40x magnification (2.0 HT Nanozoomer, Hamamatsu, Japan). Quantification of the histological composition was performed in Orbit Image Analysis (version 3.15,

Idorsia Pharmaceuticals Ltd, Allschwil). We determined the quantitative fraction (relative to the total area of the section) of: 1) fibrin fibres & platelets, 2) erythrocytes and 3) leukocytes. Fibrin fibres and platelets can not individually be distinguished using a single stain and are therefore treated as one histopathological component. Two trained observers both individually scored all samples and results were averaged. Methods used are further elaborated on in appendix C.

Statistical analysis

Reported are the stiffness values corresponding to a maximum of 75% compression, to avoid the influence of artefacts which can be expected at the transition from the loading to unloading state (at 80% compression). Additionally, the models showed an optimal fit a 75% strain. For each individual sample, stiffness values were determined from the (model fitted to the) experimental data of the initial loading cycle. A linear regression model was used to define the relation between thrombus histological components and stiffness values. Correlation strength and direction were evaluated by means of a Pearson correlation coefficient (R).

A subgroup analysis was performed by stratification of samples into four groups. Based on previous findings, which are further elaborated on in the discussion section, a significant increase in stiffness was expected for samples with a F&P content of 70-80% or higher. Therefore, samples were allocated to one of the following four subgroups, based on their fibrin & platelet content: F&P-low (0-25% fibrin & platelets), F&P moderate-low (25-50% fibrin & platelets), F&P moderate-high (50-75% fibrin & platelets) and F&P-high (75-100% fibrin & platelets). For each subgroup, a stiffness value was determined by averaging the previously calculated values of the included samples.

III. Results

21 patients were included between July and October 2019. The median age was 70 (IQR, 62-75), 38% percent was male and the median National Institutes of Health Stroke Scale (NIHSS) score was 16 (IQR, 10-20), as is shown in table I. From the included patients, 1 patient was excluded from the analysis as the retrieved thrombus material was unsuitable for testing due to the small size of the thrombus and 1 sample was excluded due to technical issues during the experiment. From the remaining 19 patients, a total of 41 samples were successfully tested, with the number of samples retrieved from each patient ranging from 1 to 4 (7 patients yielded 1 sample, 6 patients yielded 2, 2 patients yielded 3 and 4 patients yielded 4). Experimental assessment of thrombus material started within 15 minutes following the thrombectomy procedure for material retrieved of 16 out of 19 patients. Material retrieved from 3 patients (4 tested samples) was stored for a longer period of time (4, 9 and 12 hours respectively) prior to testing.

During the period of this study, several patients received full or partial treatment, yet were not included in the

Table I
COHORT BASELINE CHARACTERISTICS

Baseline characteristics	Study cohort (n=21)
Age (median, IQR)	70 (62-75)
Male sex	8 (38%)
NIHSS score on admission (median, IQR) (n=20)*	16 (10-20)
Successful reperfusion (eTICI grade 2B-3) (n=19)*	19 (100%)
Stent retriever first choice (n=20)*	20 (100%)

The baseline characteristics for the study cohort. Values are given as median and interquartile range (IQR) or as absolute value and as the percentage of the total number of reported patients.

*The parameter has only been reported for the indicated number of patients.

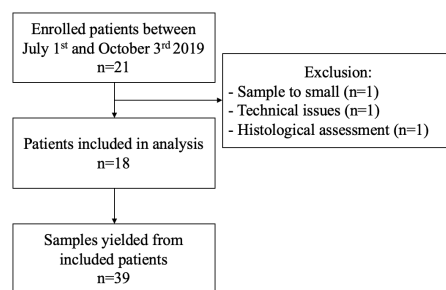


Figure 1. Flowchart representing the inclusion and exclusion of patients and samples in this study.

study as one of the inclusion criteria was not met. One patient was not included as no thrombus material had been retrieved during the procedure. Two patients have not been included due to the inability of the thrombectomy device to successfully pass the occlusion site. Two patients have not been included due to spontaneous recanalization of the occlusion during the procedure.

Histological composition

Histopathological analysis found that samples had a median of 58.9% fibrin & platelets (IQR, 36.4% - 89.8%), 40.4% RBC (IQR, 9.7% - 62.4%) and 1.1% leukocytes (IQR, 0.4% - 1.5%). Histological sections of a typical F&P low, F&P moderate-low, F&P moderate high and F&P high sample is presented in figure 2. The H&E stain colours erythrocytes red, fibrin & platelets pink and leukocytes dark purple. Two samples (harvested from 1 patient) had an abundance of cytoplasm and a relative low fibrin/platelet and erythrocyte content. Both samples were excluded due to the inability to adequately quantify these samples according to the protocol used for the analysing the data from the other samples. Further clarification in provided in appendix C. After stratification, samples sizes of the subgroup were as followed: for F/P, n=6; for F/P moderate-low, n=7; for F/P moderate-high, n=12; for F/P high, n=14.

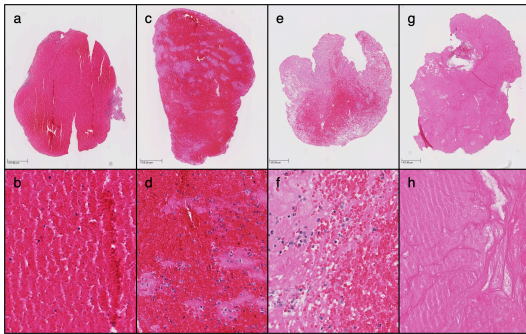


Figure 2. Histological images of a F&P low samples (a & b), F&P moderate-low sample (c & d), F&P moderate-high sample (e & f) and a F&P-high sample (g & h). Red stained tissue indicates red blood cells, fibrin/platelets are highlighted pink and leukocytes can be seen as their nucleus colours dark.

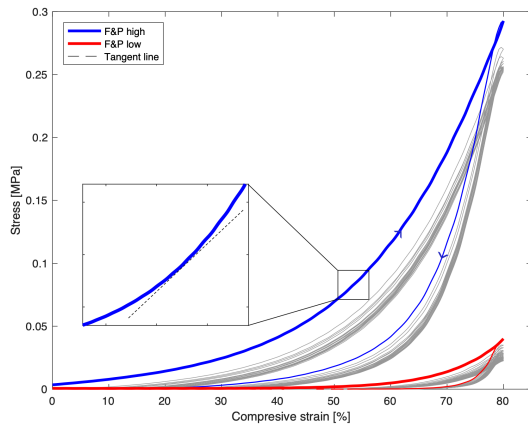


Figure 3. The initial loading and unloading curve of a fibrin & platelet high sample is represented in blue and a fibrin & platelet low sample in red. The subsequent 19 compression cycles are represented in grey for both samples. In the close up, the dashed line represents the tangent line, of which the tangent modulus can be determined by calculating the slope of that line.

Mechanical characterization

The results of an unconfined compression test are exemplified in figure 3, which illustrates typical stress-strain graphs of two samples. The initial loading and unloading cycle of a fibrin & platelet high sample and fibrin & platelet low sample are respectively marked in blue and red. The subsequent 19 compression cycles are marked in grey, for both samples. The dashed line in the close up illustrates a tangent line, of which the tangent modulus is determined by calculating the slope of the line. Assessing the initial loading curves in figure 3, which represents the first compression cycle of the thrombus (marked as the thick blue and red upward lines), it can be seen that the samples exhibit non-linearity. At low strains, the material initially behaves near linear, whilst strain stiffening occurs

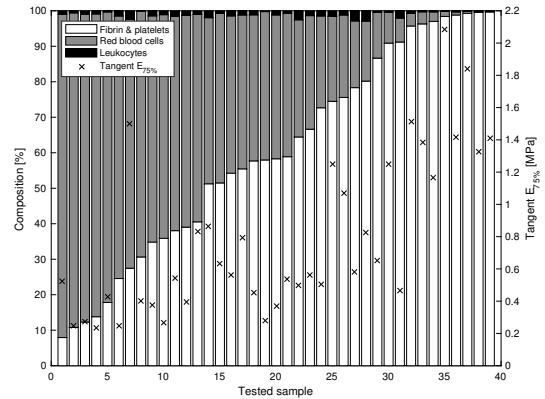


Figure 4. Histological composition of each sample is represented by the bar chart, where samples are ordered by increase in fibrin content. The corresponding tangent $E_{75\%}$ is additionally provided for each sample.

at increased compression. Although the exact transition point from the near-linear to strain-stiffening regime is not defined, it can be seen that the transition occurs at a lower strain for the fibrin & platelet high sample compared to the fibrin & platelet low sample. Furthermore, the sample's peak stress values gradually decrease for each repetitive cycle. The relative cyclic decrease in stress is more profoundly observed in the fibrin & platelet low sample compared to the high sample.

For all 39 samples, the tangent $E_{75\%}$ was determined from the initial loading curve. An averaged tangent $E_{75\%}$ of 0.78 MPa (± 0.08) was found. Figure 4 displays the composition of each sample, ordered by increase in fibrin content, and the corresponding tangent $E_{75\%}$ value. From figure 5 it can be seen that there is a positive correlation between thrombus stiffness and fibrin & platelet content ($R=0.69$, $p<0.001$). No significant correlation was found between the presence of leukocytes and thrombus stiffness ($R=-0.28$, $p>0.08$). Additional information regarding statistics can be found in appendix B.

The stiffness of each subgroup was determined at multiple strains, illustrated in figure 6. A significant increase in stiffness was found, comparing the F&P-low to the F&P moderate-high and F&P high subgroups. The stiffness values of F&P-high were significantly higher compared to the other subgroups and no significant difference was found between F&P moderate-low and F&P moderate-high. On average, F&P-high samples were 12.7 times stiffer compared to F&P-low samples at low strains (20%), and 3.7 times stiffer at high strains (75%), as can be seen in figure 6.

Material behaviour was additionally assessed over the repetitive loading cycles, by evaluating the stress corresponding to 75% strain at 1, 5, 10, 15 and 20 cycles for each group, as is shown in figure 7. The relative reduction in stress, measured as the decrease from the first cycle to both

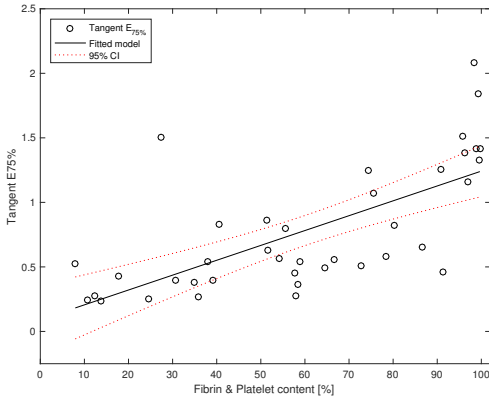


Figure 5. Linear regression of fibrin & platelet content vs. Tangent $E_{75\%}$. The 95% confidence interval lines indicate the area where it can be assumed with 95% certainty that the linear regression line will fall within, based on the provided test data.

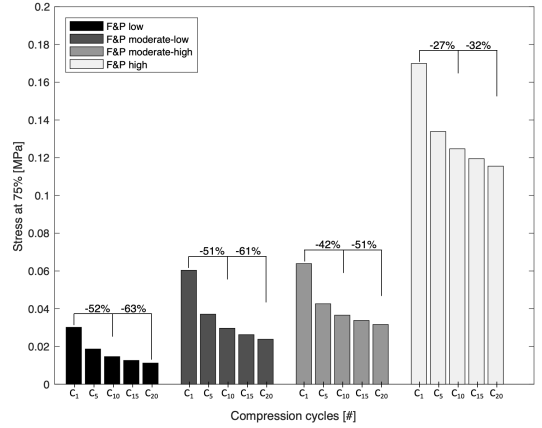


Figure 7. Averaged stress values, determined at 75% strain, for each subgroup during the 1st, 5th, 10th, 15th and 20th loading cycle. The relative decrease in stress, measured as the decrease in stress from the first to the 10th and 20th cycle, is represented by the percentages above the bars.

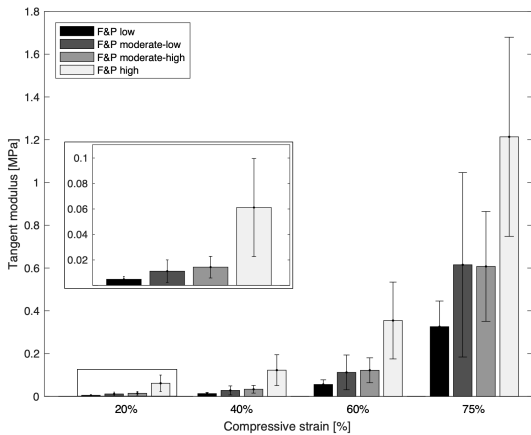


Figure 6. Derived tangent moduli for each subgroup at 20%, 40%, 60% and 75% strain. The error bars represent the standard deviation.

the 10th and 20th cycle, was approximately twice as large for F&P low samples (-53%, -63% respectively) compared to the F&P high samples (-27%, -32% respectively). Furthermore, for all subgroups it can be seen that the reduction occurs predominantly in the first 5 cycles. Within 20 cycles, the in reduction in stress approaches, though does not yet reach, stabilization.

Findings in literature

The mechanical behaviour of thrombi retrieved from AIS patients under compressive loading conditions has previously been assessed by Chueh *et al.*³ In this study, all thrombi harvested from AIS patients were retrieved

with use of aspiration techniques only. Furthermore, an alternative measure, the secant $E_{0-75\%}$, was used to describe the stiffness of their samples. The secant $E_{0-75\%}$ is defined as the slope of a line drawn from the origin of the stress-strain curve to the point on the curve corresponding to 75% strain. For comparison, the secant $E_{0-75\%}$ has been determined for the samples tested in this study.

Additionally, clot analogues have been examined by Chueh *et al.* and Malone *et al.*^{3,8} In both studies, clot analogues were created from whole blood, either with human or bovine blood and with or without the addition of thrombin. The reported stiffness values of both studies and of this study are presented in table II.

IV. Discussion

This is the first study performing a combined quantitative histopathological and a mechanical analysis on fresh thrombi retrieved from AIS patients. This resulted in four main findings. Firstly, the results showed a positive correlation between the stiffness and the quantitative fraction of fibrin & platelets of the tested samples ($R=0.69$, $p<0.001$). Secondly, from a mechanical point of view, it was found that the F&P moderate-low and F&P moderate-high group showed similar behaviour. Thirdly, based on stiffness values reported in literature, we conclude that clot analogues used in mechanical experiments most accurately resemble the soft and fibrin & platelet low thrombi found in this study. Lastly, non-linear and viscoelastic behaviour was exhibited by all samples.

Our first conclusion is that the results of this study indicate that thrombus mechanical properties are related to composition. An increase in fibrin & platelet content has shown to result in an increased stiffness, which can lead to an order of magnitude in difference comparing fibrin

Table II
STIFFNESS VALUES OF AIS THROMBI AND CLOT ANALOGUES

AIS thrombi	Tangent $E_{40\%}$ [MPa]	Secant $E_{0-75\%}$ [MPa]
<i>Study</i> - F&P low	0.013	0.039
<i>Study</i> - F&P moderate-low	0.028	0.077
<i>Study</i> - F&P moderate-high	0.033	0.082
<i>Study</i> - F&P high	0.123	0.332
<i>Chueh</i> - undefined	-	0.04
Clot analogues		
<i>Chueh</i> - Human WB	-	0.01
<i>Chueh</i> - Human WB + thrombin	-	0.02
<i>Chueh</i> - Bovine WB	-	0.05
<i>Chueh</i> - Bovine WB + thrombin	-	0.065
<i>Malone</i> - Bovine WB + thrombin	0.014	-

The stiffness values determined for thrombi retrieved from AIS patients in this study and reported by *Chueh et al.* *Chueh et al.* does not provide a quantitative measure the composition of their samples, however they are classified as being "red". Additionally, reported stiffness values determined for whole blood (WB) clots, assessed by *Chueh et al.* and *Malone et al.* are presented. The tangent $E_{40\%}$ and the secant $E_{0-75\%}$ are two independent measures for stiffness and can not directly be compared to each other. Therefore both measure have been provided for the samples assessed in this study.

& platelet high to fibrin & platelet low samples. However, it should be pointed out that, although fibrin & platelet content seems to be a strong influencing factor, other factors will additionally effect the mechanical properties, causing for the variation observed within the test data. One such factor could be the ratio at which fibrin and platelets are present, which is currently unknown for the tested samples. It has been shown that platelets are the key drivers for clot contraction and it is highly plausible that contraction will effect the mechanical properties of a thrombus.^{9,10} If so, then additionally the stage of contraction, independent of the composition or ratio of fibrin to platelets, will furthermore influence thrombus mechanical properties. To date, the limited research on the mechanical properties of AIS thrombi has been performed by *Chueh et al.*, who investigated nine thrombi retrieved from four AIS patients. The composition of the samples was not quantitatively determined, however the samples were histologically assessed and qualitatively categorized as "red".³ They reported an average secant $E_{0-75\%}$ of 0.040 MPa for these specific thrombi, which is in the range of the secant $E_{0-75\%}$ values determined of the F&P low subgroup, as is shown in table II. Therefore, we can suggest that the thrombi assessed by *Chueh et al.* do not resemble the full spectrum of those found in vivo, as the extensive range in composition and mechanical properties of thrombi has been demonstrated in this study (table II). A bias has likely been introduced (in the study of *Chueh et al.*) towards one type of thrombus, attributable to the small samples size and the use of aspiration as the only retrieval method. Therefore, the results of this study add to what has already been reported in literature, due to the large diversity in both composition and mechanical behaviour of the included

samples.

Secondly, we can conclude that, from a mechanical point of view, behaviour was very similar for the F&P moderate-low and F&P moderate-high subgroups. At low fibrin/platelet contents (0-25%), samples have a low stiffness and are susceptible to a large decrease in peak stress values over repetitive loading. Stiffness increases at an intermediate fibrin/platelet content, between 25%-75%. Yet for the samples allocated to the F&P moderate-low and F&P moderate-high group, the exact composition was of little influence on a samples mechanical behaviour, as the stiffness was found to be comparable for both groups. However, at a fibrin/platelet content above 75%, stiffness significantly increases and the relative reduction in stiffness caused by repetitive loading is only half as large compared to the F&P low group. Previous studies have assessed clot analogues, under various loading conditions, by means of combined microstructural and mechanical analyses. It was found that an increase in red blood cell content disrupts the integrity of the fibrin structure as fibre density gradually decreases, thereby altering clot stiffness, elastic and viscoelastic properties.^{4,5,6,7} *Gersh et al.* performed rheometric experiments on analogues made from solutions with 0%, 10%, 20%, 40% and 50% red blood cell content. A significant change in behaviour was observed comparing the 0% to 20% analogues, as the clots became more viscous, rather than elastic, due to the exposure of erythrocytes. However, at further increased red blood cell contents, the behaviour was similar to that of the 20% RBC analogues.⁴ Although the exact composition of the analogues examined by *Gersh et al.* is not known (only the haematocrit of the blood mixture) and the experimental technique used is different compared to unconfined compression, the observed trend is in agreement with the results found in this study, as stiffness significantly increases for samples with fibrin & platelet content increasing above 70%-80%. Based on the microstructural analysis of *Gersh et al.*, the influence of red blood cells within a fibrous network seem to be most pronounced when introduced in a fibrin rich clot. It can be suggested that it is in these fibrin rich thrombi that the reduction in fiber density has the strongest impact on inter-fiber bonds, which strongly contribute to the strength and rigidity of fibrin fiber networks.^{11,12} Potentially, at a fibrin & platelet content below 70% to 80%, fibrin fibers can no longer sufficiently create inter-fiber bonds due to the disruption of the red blood cells in the network, merely serving as individual connectors between erythrocytes. Additional mechanical and microscopical analyses of analogues with histopathologically verified compositions might provide evidence to why it is observed.

Thirdly, the mechanical behaviour of clot analogues under compressive loading conditions was assessed by *Chueh et al.* and *Malone et al.*^{3,8} Analogues were made from whole blood, with and without the addition of thrombin. Their reported stiffness values are presented in table III, where it can be seen that the stiffness values of all analogues fall within the range of the F&P low group. Furthermore, whole blood (in fluid state) consists of approximately 40% red

blood cells.¹³ It has been shown that coagulation of a solution containing 40% red blood cells, under static conditions and with the addition of clotting agents, results in a thrombus consist of approximately 30%-40% fibrin/platelets.¹⁴ Assuming this holds for the whole blood analogues created by *Chueh et al.* and *Malone et al.*, the results show that their whole blood analogues have a lower stiffness compared to retrieved thrombi with a similar haematocrit, as these clots should resemble those of the F&P moderate-low subgroup. Thus, it has become evident that analogues created using the procedure described in these papers are from a mechanical perspective- not representative for fibrin-rich clots.

Lastly, in agreement with literature, it was found that thrombi exhibit non-linear behaviour, as an increase in strain results in an increased stiffness. The extent of this non-linearity is composition dependant and of great influence on thrombus-stent interactions, as the force required to compress or penetrate a thrombus will increase at depth. Furthermore, although not addressed in literature, the viscoelastic behaviour of the tested samples can be observed from the stress-strain graphs (figure 3). Firstly, as has previously been mentioned, there is a change in response to the subjected load after each cycle. Secondly, the unloading curve does not follow the same trajectory as the loading curve. This phenomenon, called hysteresis, is generally caused by material viscous properties and provides information regarding a material's time-dependant behaviour. However, additional influencing factors arise as a result of the relatively large deformation applied in this experiment, including the change in sample volume and permanent damage occurring to the samples structure. Therefore, it would be unsuitable to quantify the viscoelastic behaviour based on this experiment alone. Additional experiments, including rheometric, stress-relaxation and creep test, could provide measures for the additional factors. Multiscale models, which can account for the various influencing factors, would allow for a more appropriate description of both the non-linear and viscoelastic behaviour. Nevertheless, these observations provide direction in describing the differences in non-linear and viscoelastic behaviour between fibrin rich and fibrin poor thrombi.

Clinical relevance

Both clinical and in vitro studies have provided evidence that fibrin rich thrombi are associated with an increased number of passes and lower retrieval success rates.^{2,15,16,17} As a thrombectomy procedure largely depends on the mechanical interactions between the thrombus and device, the results of this study assist in supporting the previously found relation, by assessing thrombi from a mechanical and histological point of view.

Furthermore, it has been found that analogues assessed in literature, generally created from whole blood, often only resemble the soft, fibrin poor thrombi. However, it seems that fibrin rich thrombi are most difficult to retrieve and

should therefore be of greatest interest to research. As clot analogues are used both for experimental mechanical characterization and by industry for assessment of thrombectomy devices, it is of importance that they represent the full spectrum of in vivo thrombi from a mechanical point of view, including those that are fibrin rich. Data gathered in this study can be used as a reference in the creation of representative thrombus analogues.

Considering the large variety in mechanical behaviour between the tested samples, one could argue that a single type of stent design does not suffice for all types thrombi. Based on the previously reported results it could be suggested that a set of three devices, each with specific properties, would be required to retrieve all the samples in the F&P low, F&P moderate-low and -high and F&P high groups. This thrombus-specific retrieval approach requires prior knowledge on thrombus mechanical properties. Although currently not yet fully validated or developed, methods for *in vivo* assessment of thrombus composition or mechanical properties are being investigated. For example, imaging techniques are utilised to determined thrombus composition by assessing clot radiodensity and ultrasound applications allow for the *in vivo* determination of mechanical properties.^{7,18,19,20} Although these techniques are not yet reliable enough to be used in practice, it is plausible that they will assist the thrombus-specific retrieval approach in the near future.

Lastly, modelling applications can contribute significantly to the improvement of analogues, thrombectomy devices and procedures by simulating in *in vivo* situations. The mathematical equations derived from the fitted models allows others to simulation of the compressive behaviour of four thrombi representing the four subgroups. Derived material constants can be found in appendix D.

It should briefly be mentioned that this study has not analysed the relation between clinical parameters and the mechanical properties of tested sample. Thrombi can be highly heterogeneous and it is uncertain to what extent a tested sample is representative for the entire thrombus. Furthermore, it is unknown what part of the thrombus has interacted with the thrombectomy device. Therefore, the relation between clinical parameters, and the mechanical behaviour of tested samples can not directly be made.

Limitations

The authors acknowledge that there are several limitations to this work. Patients for whom thrombus material could not be retrieved were not included in this study. Therefore, it is plausible that the most difficult to retrieve thrombi have not been included in this study. Additionally, due to the relatively small number of included patients, it is uncertain whether the tested samples represent the full range of thrombi potentially found in vivo.

Furthermore, certain samples could not be tested due to their inability to remain intact during handling, potentially introducing a bias. It was observed that stiffer, fibrin rich thrombi allowed for easier handling and an increased number of successful experiments per patient.

Nevertheless, the number of tested samples in this study is considerably larger compared to current literature and with the good histological distribution (fibrin & platelet content ranging from 7% to 99%, figure 4) we expect to have covered a substantial range of thrombi found *in vivo*.

V. Conclusion

In summary, a positive correlation was found between thrombus stiffness and fibrin & platelet content ($R=0.69$, $p<0.001$). Furthermore, from a mechanical point of view, there was little difference between thrombi in the F&P moderate-low and F&P moderate-high group. Additionally, whole blood thrombus analogues, often reported in current literature, most accurately resemble soft, fibrin poor samples. However, these thrombi fail to represent the wide range of thrombi found *in vivo*. Lastly, it was found that all thrombi exhibited non-linear and viscoelastic behaviour. The results of this study can be used for the improvement of clot analogues and for further modelling applications.

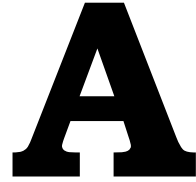
References

- ¹ Simon F De Meyer, Tommy Andersson, Blaise Baxter, Martin Bendszus, Patrick Brouwer, Waleed Brinjikji, Bruce CV Campbell, Vincent Costalat, Antoni Dávalos, Andrew Demchuk, et al. Analyses of thrombi in acute ischemic stroke: a consensus statement on current knowledge and future directions. *International journal of stroke*, 12(6):606–614, 2017.
- ² Sharon Duffy, Ray McCarthy, Michael Farrell, Sunitha Thomas, Paul Brennan, Sarah Power, Alan O’Hare, Liam Morris, Eleanor Rainsford, Eugene MacCarthy, John Thornton, and Michael Gilvarry. Per-Pass Analysis of Thrombus Composition in Patients With Acute Ischemic Stroke Undergoing Mechanical Thrombectomy. *Stroke*, 50(5):1156–1163, may 2019.
- ³ J Y Chueh, A K Wakhloo, G H Hendricks, C F Silva, J P Weaver, and Matthew J Gounis. Mechanical characterization of thromboemboli in acute ischemic stroke and laboratory embolus analogs. *American Journal of Neuroradiology*, 32(7):1237–1244, 2011.
- ⁴ Kathryn C Gersh, Chandrasekaran Nagaswami, and John W Weisel. Fibrin network structure and clot mechanical properties are altered by incorporation of erythrocytes. *Thrombosis and Haemostasis*, 102(6):1169–1175, 2009.
- ⁵ Fiona M Weafer, Sharon Duffy, Ines Machado, Gillian Gunning, Pasquale Mordasini, Ellen Roche, Peter E. McHugh, and Michael Gilvarry. Characterization of strut indentation during mechanical thrombectomy in acute ischemic stroke clot analogs, 2019.
- ⁶ N Tynngard, T Lindahl, S Ramstrom, and G Berlin. Effects of different blood components on clot retraction analysed by measuring elasticity with a free oscillating rheometer. *Platelets*, 17(8):545–554, 2006.
- ⁷ Chih Chung Huang, Pay Yu Chen, and Cho Chiang Shih. Estimating the viscoelastic modulus of a thrombus using an ultrasonic shear-wave approach. *Medical Physics*, 40(4), 2013.
- ⁸ F Malone, E. McCarthy, P Delassus, P Fahy, J Kennedy, A J Fagan, and L Morris. The Mechanical Characterisation of Bovine Embolus Analogues Under Various Loading Conditions. *Cardiovascular Engineering and Technology*, 9(3):489–502, 2018.
- ⁹ Douglas B Cines, Tatiana Lebedeva, Chandrasekaran Nagaswami, Vincent Hayes, Walter Masselski, Rustem I Litvinov, Lubica Rauova, Thomas J Lowery, and John W Weisel. Clot contraction: compression of erythrocytes into tightly packed polyhedra and redistribution of platelets and fibrin. *Blood*, 123(10):1596–1603, 2014.
- ¹⁰ Akiko Ono, Erik Westein, Sarah Hsiao, Warwick S Nesbitt, Justin R Hamilton, Simone M Schoenwaelder, and Shaun P Jackson. Identification of a fibrin-independent platelet contractile mechanism regulating primary hemostasis and thrombus growth. *Blood*, 112(1):90–99, 2008.
- ¹¹ Christine R Carlisle, Eric A Sparks, Christelle Der Loughian, and Martin Guthold. Strength and failure of fibrin fiber branchpoints. *Journal of Thrombosis and Haemostasis*, 8(5):1135–1138, 2010.
- ¹² W Liu, CR Carlisle, EA Sparks, and Martin Guthold. The mechanical properties of single fibrin fibers. *Journal of Thrombosis and Haemostasis*, 8(5):1030–1036, 2010.
- ¹³ Himel Mondal, Deepa Budh, Rhonda Coffman, Lindsay Iverson, and Heather Templin. Hematocrit (hct). *Stat-Pearls*, 2019.
- ¹⁴ Sharon Duffy, Michael Farrell, Kevin McArdle, John Thornton, David Vale, Eleanor Rainsford, Liam Morris, David S Liebeskind, Eugene MacCarthy, and Michael Gilvarry. Novel methodology to replicate clot analogs with diverse composition in acute ischemic stroke. *Journal of NeuroInterventional Surgery*, 9(5):486–491, 2017.
- ¹⁵ Kota Maekawa, Masunari Shibata, Hideki Nakajima, Akane Mizutani, Yotaro Kitano, Masaru Seguchi, Masayoshi Yamasaki, Kazuto Kobayashi, Takanori Sano, Genshin Mori, Tadashi Yabana, Yutaka Naito, Shigetoshi Shimizu, and Fumitaka Miya. Erythrocyte-rich thrombus is associated with reduced number of maneuvers and procedure time in patients with acute ischemic stroke undergoing mechanical thrombectomy. *Cerebrovascular Diseases Extra*, 8(1):39–49, 2018.
- ¹⁶ Ichiro Yuki, I Kan, H V Vinters, R H Kim, A Golshan, F A. Vinuela, J W Sayre, Y Murayama, and F Vinuela. The impact of thromboemboli histology on the performance of a mechanical thrombectomy device. *American Journal of Neuroradiology*, 33(4):643–648, 2012.
- ¹⁷ Jong Wook Shin, Hye Seon Jeong, Hyon Jo Kwon, Kyu Sang Song, and Jei Kim. High red blood cell composition in clots is associated with successful recanalization during intra-arterial thrombectomy. *PLoS ONE*, 13(5):e0197492, may 2018.
- ¹⁸ Natasha Simons, Peter Mitchell, Richard Dowling, Michael Gonzales, and Bernard Yan. Thrombus composition in acute ischemic stroke: a histopathological study of thrombus extracted by endovascular retrieval. *Journal*

of Neuroradiology, 42(2):86–92, 2015.

¹⁹ David S Liebeskind, Nerses Sanossian, William H Yong, Sidney Starkman, Michael P Tsang, Antonio L Moya, David D Zheng, Anna M Abolian, Doojin Kim, Latisha K Ali, et al. Ct and mri early vessel signs reflect clot composition in acute stroke. *Stroke*, 42(5):1237–1243, 2011.

²⁰ Hua Xie, Kang Kim, Salavat R Aglyamov, Stanislav Y Emelianov, Matthew ODonnell, William F Weitzel, Shirley K Wroblewski, Daniel D Myers, Thomas W Wakefield, and Jonathan M Rubin. Correspondence of ultrasound elasticity imaging to direct mechanical measurement in aging dvt in rats. *Ultrasound in medicine & biology*, 31(10):1351–1359, 2005.



Mechanical force tester

A.1. Materials and setup

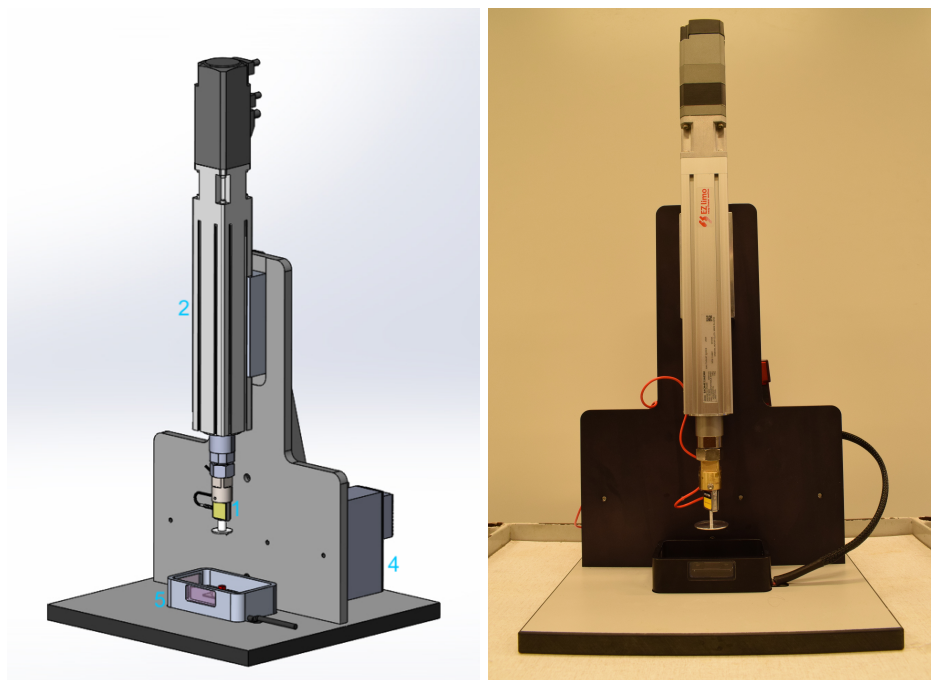
In order to assess the Stress-strain behaviour of thrombus samples, a customized force tester was built, as both hardware and software could be tailored to specific requirements of the experiment. Based on reported literature, expected stress and strain values were used to determine the optimal configuration for measurements at both small and large strains. The force tester consists of five main components: The setup and specifications are presented in figure [A.1](#).

The S-beam loadcell operates according to the strain gauge principle, in which the deflection of a beam in the loadcell causes for an increased or decreased resistance of the excitation voltage, leading to a change in output signal. The output signal is transformed to a $\pm 10V$ signal with use of the amplifier.

The Labjack U6-pro data acquisition device allows for the conversion from analogue input signals to a digital output and vice versa. With use of the data acquisition device, computer software can be used to read out the signal provided by the loadcell and to control the linear actuator.

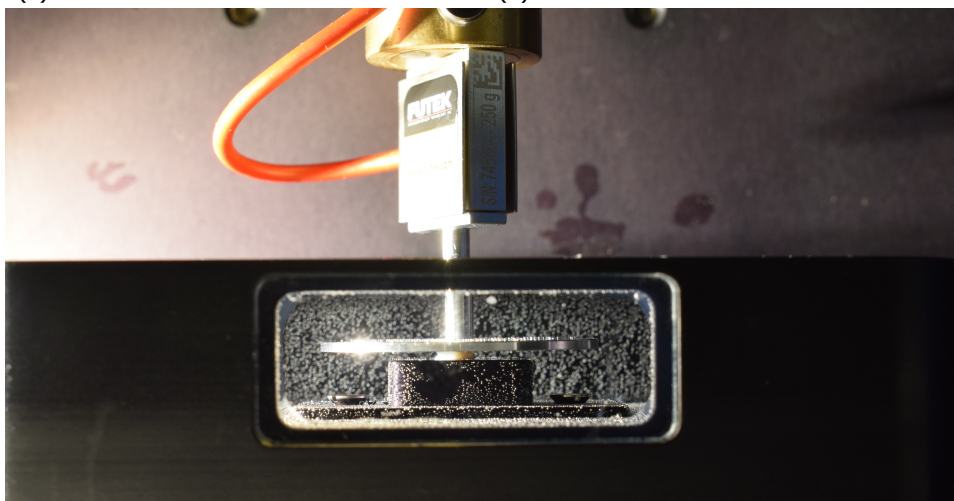
The actuator is a stepper motor and has a resolution of 0.01mm, stroke length of 150mm, maximal vertical thrust force of 200N. It consisted of an electromagnetic brake, preventing unintentional vertical movement during a power cut, and an integrated controller which accommodates 10 digital inputs and 6 digital outputs. Manual control and loading of actuation profiles can be done through the accommodated MEXE02 software. The integrated controller allows for activation of pre-defined actuation profiles and a selection of actions through alternative software.

The heated basin is controlled by a self-regulating temperature system.



(a)

(b)



(c)

Figure A.1: **Mechanical force tester.** (a) Technical drawing, (b) front view image, (c) Front view during a compression experiment.

1. 250g s-beam loadcell (LSB200 Jr. Miniature S-beam loadcell, Futek)
2. Linear actuator (EACM4-E15-AZMK, Oriental motor)
3. Amplifier – TXDIN1600s (Omega/status instruments)
4. Data Acquisition device (U6-pro, Labjack)
5. Heated container – In-house build

A.2. Software

MEXE02 and *LabVIEW* software were used to operate the force tester and acquire data from the loadcell simultaneously.

MEXE02

The *MEXE02* software allows the user to drive the motorized cylinder manually. Alternatively, one can initiate a pre-defined action, for which the operational settings (operating -mode, -position, -speed, -current, acceleration speed, delays, loop counts and more) are defined. Sequential actions can be run automatically, creating an operating profile in which the individual actions run according to their specific settings. When assigned to the controller, the single actions or operating profiles can be initiated either through the *MEXE02* software or by excitation of the digital input channels of the integrated controller. An interface created in *LabVIEW* provided a standardized protocol for operation of the tester and a live read out of the loadcell.

LabVIEW

LabVIEW allows the user to create and run interactive digital applications and simulations, of which the inputs and outputs are controlled and graphically visualized in a customized interface. *LabVIEW* was used to operate and visualize the digital and analogue in-/output channels of the DAQ device. Graphical coding is performed in the block diagram, represented in (figure A.2) The interface (figure A.3) graphically visualized real-time data generated by the loadcell and allowed for the initiation of the following actions and operating profiles of the actuator:

- Raise of the compression plate to upper most position
- Lowering of the compression plate to the starting position (as defined in *MEXE02*)
- Taring of the loadcell
- Starting the compression experiment (as defined in *MEXE02*) and recording of the loadcell input
- Aborting the current action or operation.

A.3. Validation

Loadcell accuracy

Accuracy of the loadcell was assessed with use of calibrated weights, ranging from 1g to 250g. Table A.1 shows the obtained results. The measured error was largest in the lower range, with an error of 2.7% at a load of 1 g.

Validation of the experimental setup

The mechanical force tester has been validated as one assembled unit by means

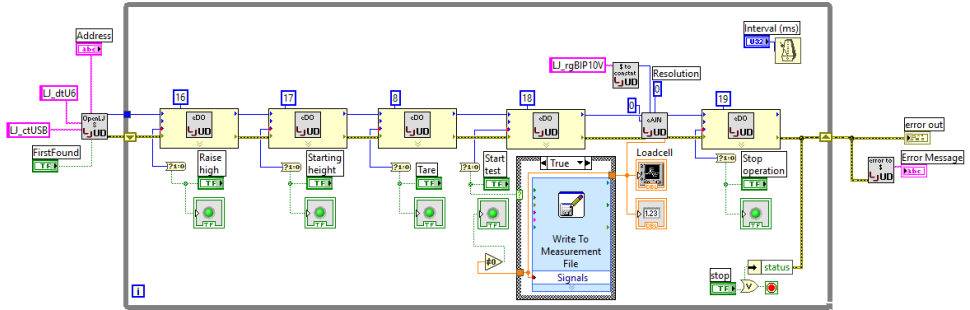


Figure A.2: **Block diagram in LabVIEW: graphical code created to run the front panel in LabVIEW. The data acquisition device is linked to LabVIEW, allowing for the transmission of both analogue and digital inputs and outputs between the force tester and the laptop.**

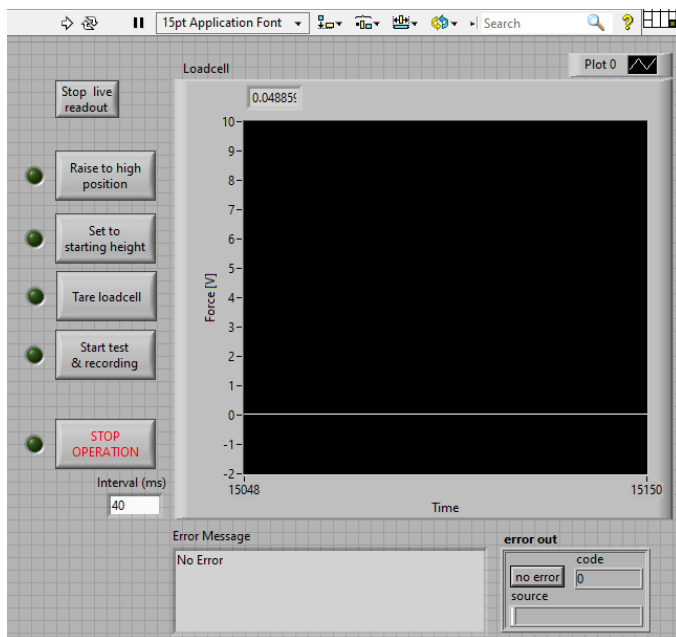


Figure A.3: **Front panel in LabVIEW: The graphical user interface used to operate the force tester and provide a live readout of the loadcell.**

Table A.1: Loadcell accuracy

Calibration weight [g]	Expected readout [V]	Loadcell readout [V]	Error [V]	Error [%]
1	0.04	0.041	0.001082	2.71
2	0.08	0.082	0.001833	2.29
5	0.2	0.202	0.001897	0.95
10	0.4	0.403	0.003125	0.78
20	0.8	0.805	0.004654	0.58
50	2	2.005	0.004753	0.24
100	4	4.008	0.008402	0.21
200	8	8.023	0.023156	0.29
250	10	10.024	0.024300	0.24

Expected and measured values for the validation of the loadcell with use of calibrated weights.

of a controllable and repeatable experiment. A compression test was performed on four springs with varying stiffnesses. Springs were chosen as a test material as, when subjected to compressive loads, their stress-strain response is linear, not time dependent and (to a great extent) does not change over repetitive loading. This allowed for the repetition of the experiment at multiple locations at varying points in time. The spring constant (k) was determined for each spring, according to the following formula:

$$k = \frac{\Delta F}{\Delta l} \quad (\text{A.1})$$

Where F is the applied force and l the length of the spring. In order to validate the system, the spring constants of a unique set of springs was determined with calibrated force testers, located at 1) the Biomechanical engineering department at the TU Delft (Lloyd instruments LR 5K, 5N loadcell), 2) NUIG Galway, Ireland (Zwick roell ..). Each spring was loaded twice according to the same protocol and the average k of the two runs was taken. The results are shown in table A.2.

Fluid displacement

As experiments are conducted with the samples submerged, additional forces come in to play which need to be accounted for. (Partially) submerging an object results in the displacement fluid, of which the volume is similar to that of the submerged object. In a small semi-confined environment (such as a basin), the medium level will rise and due to the gravitational forces, pressure will be exerted on the object. During the experiment, the compression head moves downward, increasing the volume of displaced medium, which in this setup will result in a compressive force on the load cell. To minimize this effect, rather than using a solid cylindrical compression head, a thin plate was used which was attached to the loadcell with a small diameter connector beam. Therefore, the volume of medium displaced during

Table A.2: Loadcell accuracy

	<i>k</i> values			
	Spring 1	spring 2	spring 3	spring 4
Force tester	84.4	714.2	101.1	2700.9
TU delft	82.3	714.8	100.1	2821.2
Cerenovus, Galway	82.7	705.2	99.8	2719.5

Spring stiffness (*k*) values determined for four individual springs. *k* was determined at 2 alternative locations in order to validate accuracy of the machine as a whole.

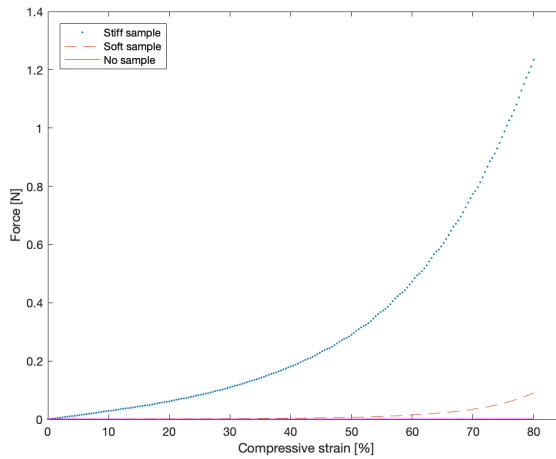


Figure A.4: **A force-displacement graph, showing the results of standard test on a stiff sample, a soft sample and without the sample. All tests are performed with the compression plate submerged.**

the experiment is largely reduced, minimizing the above described effect.

A compression experiment was executed according to the standard protocol, without the use of an sample, to measure the forces induced due to fluid displacement. Figure A.4 shows the result of the executed test without a sample, with a stiff sample and with a soft sample.. It can be seen that the effect of volume displacement is negligible in comparison to forces at strains above.

B

Collection, preparation and testing of thrombus samples

B.1. Thrombus collection and preparation

A collection protocol was set up in collaboration with the intervention radiology department to ensure thrombi could be collected directly following retrieval. In practice, multiple attempts are often required to achieve full recanalization, as initial attempts are often not or partially successful. Therefore, the material retrieved during each attempt was collected in an individual container, for a future retrospective per-pass analysis.

Specimens used for (unconfined) compression tests are often cylindrically shaped and consist of a flat top and bottom surface, as this allows for standardized derivation of stress and strain values without the need of computational modelling and finite element simulations. To create such a sample, a trimming fixture was designed which consists of multiple slits, allowing to trim a section of the thrombus to a length of 1, 2, 3, 4 or 5mm (figureB.1). The trimming fixture was used to create samples with a standardized height and consisting of a flat top and bottom surface. To minimize the risk of the sample buckling or tipping over during compression, a high aspect ratio is desirable. Assessing both clot analogues and human samples, it was found that trimming samples to a height of 1mm was most optimal to accompany each sample with the dimensions suitable for compression testing. From each thrombus, after a suitable sample was trimmed, an additional sample was cut from the remaining tissue directly adjacent to the test sample. This sample was fixated in glutaraldehyde to preserve it for evaluation with a scanning electron microscope in a retrospective study.

Thrombus material was photographed at multiple stages before and after trimming under controlled conditions. This was achieved with an enclosed lighting setup and a protocol for standardized camera settings. Samples were photographed next

to a ruler, providing a dimensional reference (include figure of lighting setup).

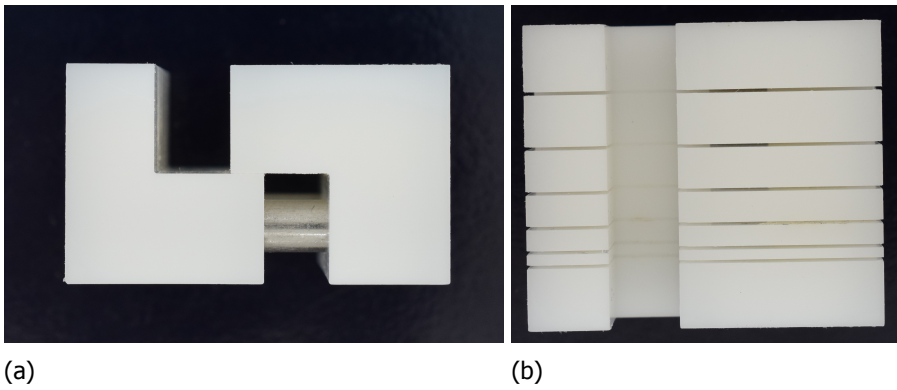


Figure B.1: **The trimming fixture used to cut the sample to the desired height. Available dimensions were 1mm, 2mm, 3mm, 4mm and 5mm. (a) Sideview of the trimming fixture. (b) Topview of the trimming fixture.**

B.2. Unconfined compression test

An unconfined compression test was chosen to determine the material properties of thrombi for the following reasons: 1) It is a standardized experimental method which has been successfully used for the analysis of soft biological tissue. 2) It is the only test method previously used to determine the mechanical properties of AIS samples, allowing for comparison to literature. 3) It is being applied by collaborators of the INSIST consortium to determine the mechanical properties of clot analogues under similar conditions. Performing a similar experiment in identical conditions allows for the direct comparison of results. 4) A thrombus is subjected to compressive loads at multiple stages during the occlusion of the vessel and recanalization of the artery. Therefore, determining the properties under subjective loads illustrates the mechanical behaviour of the thrombus during critical parts of both occlusion and recanalization of the artery.

During an unconfined compression test, the sample is placed on a stiff and impermeable surface. A load is applied vertically on the sample by compression the sample between the bottom surface and a compression plate. There are no constraints for the sample to expand in the radially. Furthermore, zero friction is assumed between the sample and the top and bottom surface. Although zero friction can not be achieved in practice, the test environment, with the sample submerged in medium, promotes the reduction of friction.

B.2.1. Compression profile

After preparation of the sample, the thrombus was placed in the basin and the compression plate lowered to the starting height of 1.1 mm above the base. As the samples were cut to 1 mm in height, this provided margin of 0.1mm to start out of contact. With both the sample and plate submerged, an adequate period of time was waited before starting the test, to allow for both the sample as the plate to reach a temperature of 37° C. As soon as the read-out value of the loadcell had stabilized, the loadcell was tared and the test started.

The following steps were executed by the actuator after initiation of the compression test in LabVIEW:

- 1 second hold period - The holding period was introduced to allow for a potential lag within the data acquisition software during the initiation of actuator movement. This initial second is removed from the analysed data.
- 80% compression, at a strain rate of 0.1mm/s
- 80% retraction, at a strain rate of 0.1mm/s
- Repetition of the cycle, 20 times

The sampling rate was set at 25 Hz.

B.2.2. Data analysis

The amplified readout of the loadcell was recorded in volts (V), provided as a function of time. The applied force, F in newtons (N) was determined according to the following formula (figure ...):

$$\text{Value}_N = \text{Value}_V * 0.25 \quad (\text{B.1})$$

In order to compare samples with different dimensions, the applied stress, σ , was determined for each sample(figure ...). Nominal stress is denoted as followed:

$$\sigma = \frac{F}{A} \quad (\text{B.2})$$

Where F is the applied force in newton and A the initial cross-sectional area of the sample in m^2 . As the samples are not perfectly cylindrical, the cross-sectional area can not be simply determined with use of the diameter. Therefore, an image of the sample (before testing) next to a ruler was used to calculate the cross-sectional area with ImageJ software. The ruler is provides a dimensional reference which is used to determine the pixel to length ratio. An example is provided in figures B.2a and B.2b. Stress (σ) as a function of strain (ϵ) was determined by dividing the maximum strain by the total number of samples corresponding to a full loading cycle. It was found that each sample corresponds to 0.4% compression. Stress is then plotted as a function of strain (figure ...)

The resulting stress values were used for further derivation of mechanical properties, such as the secant and tangent modulus. To address the non-linear behaviour, the tangent model provides a more accurate measure of the stiffness. However, both moduli were determined in order to compare with reported stiffness values in literature. Derivation of both moduli is further discussed in chapter D.1

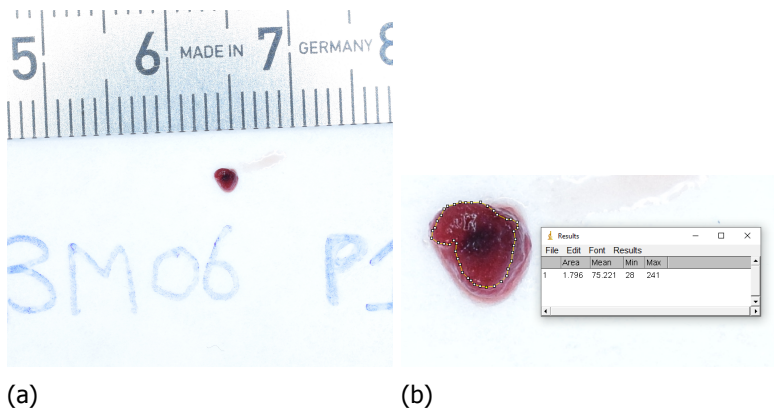


Figure B.2: (a) Photograph taken of a sample next to a ruler, after trimming and before testing. (b) Processing of the image in ImageJ software to determine the sample's cross-sectional area. The ruler (not visible in this image) is used to determine the pixel-to-length ratio.

B.2.3. Results

For each sample, the secant and tangent moduli were determined from the models fitted to the initial loading curve, at multiple strains ranging from 5% to 80%. The secant $E_{0-75\%}$ and tangent $E_{75\%}$ are represented in figures B.3a and B.3b. A similar trend can be seen for both measures of stiffness. Figures B.4a-c show the linear regression models between the stiffness values and (a) Fibrin/platelet content, (b) Red blood cells and (c) Leukocytes. Pearson's correlation coefficient was determined for each of the models, presented in table B.4d. Due to the relatively low amount of leukocytes, RBC content is dependant of Fibrin&Platelet content. Therefore, it is expected that the Pearson's correlation coefficient between stiffness and RBC is similar, but negative, compared to that between stiffness and Fibrin&platelet content. Furthermore, not finding a significant correlation between stiffness and leukocyte content corresponds with the observed results.

The tangent and secant moduli, measured at strains ranging from 5%-80%, are represented in figure B.5 for all four subgroups. As discussed in the Chapter 1, it can be seen that the F&P low group has a lower stiffness compared to the other three groups. Both F&P moderate groups have similar stiffness, which is higher compared to the F&P low group. The F&P high group is significantly stiffer compared to the other three groups, over the entire range of stiffness.

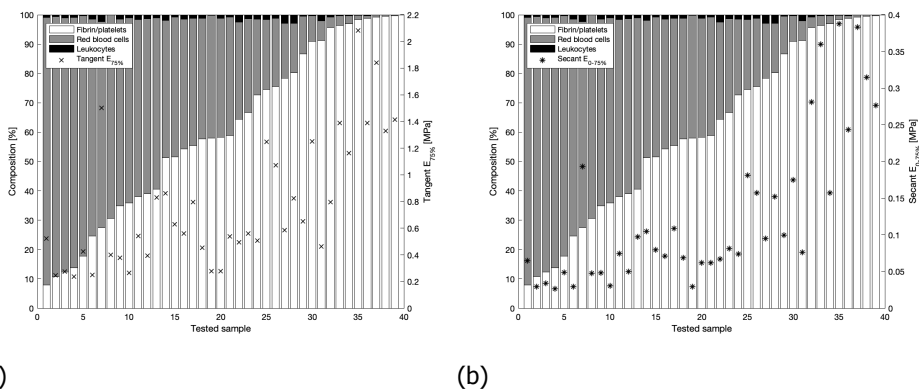


Figure B.3: **Histological composition of each sample is represented by the bar charts, where samples are ordered by increase in fibrin content. For each sample, the corresponding tangent $E_{75\%}$ (a) and secant $E_{0-75\%}$ (b) are additionally provided for each sample.**

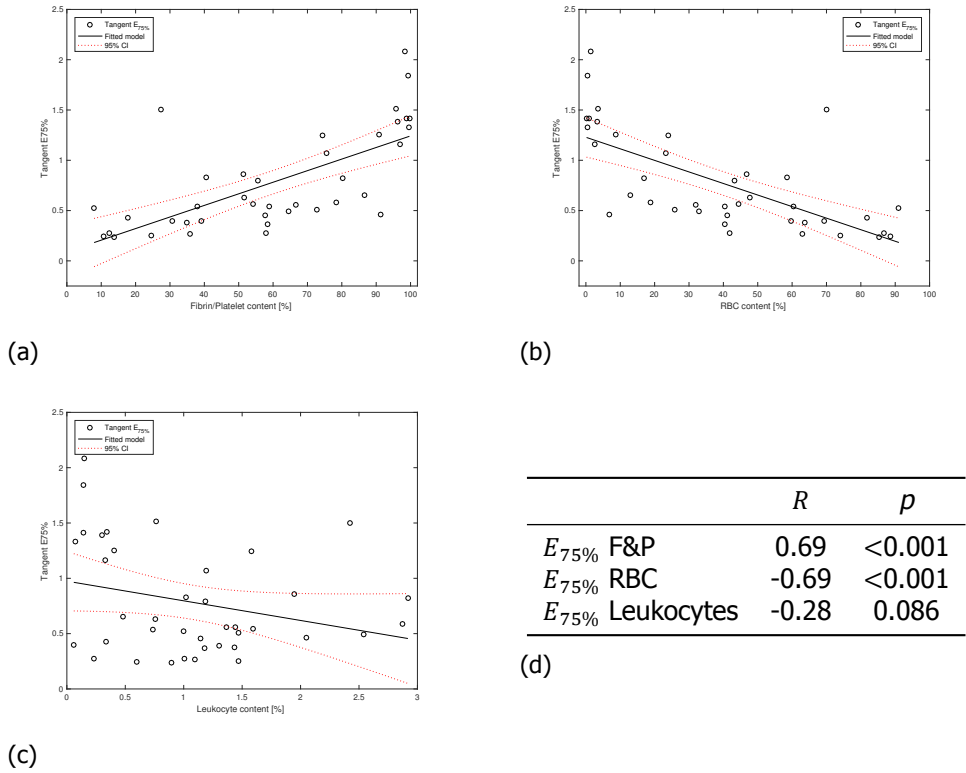


Figure B.4: Linear regression model between sample stiffness (determined as the tangent modulus at 75%) and (a) Fibrin & platelet content, (b) Red blood cells and (c) Leukocytes. Pearson's correlation coefficient (R_s) and significance p are provided for the correlation between the measured stiffness and histological component is (d).

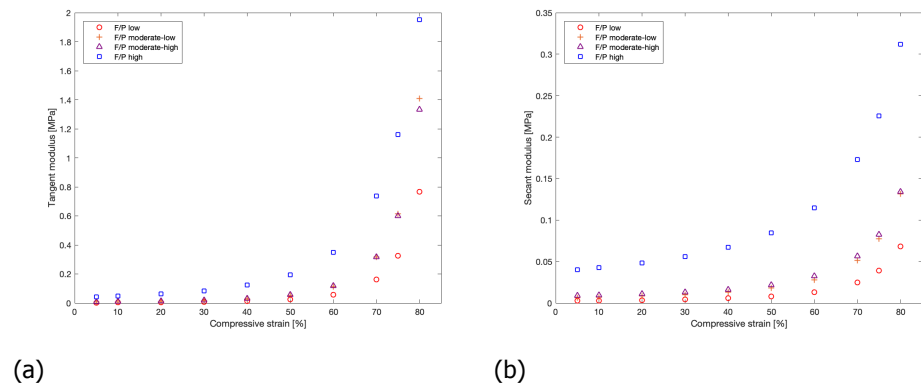


Figure B.5: Derived tangent moduli (a) and secant moduli (b) for all subgroups at increasing strains, ranging from 5% to 80%

C

Histology

C.1. Methods

Fixation

Following the unconfined compression test, each sample was placed in a cassette and chemically fixated in 3.7-4.2% buffered formaldehyde (place image). Fixation is a technique where crosslinks are chemically formed between the proteins and lipids of biological material. It is required to prevent autolysis and to preserve the tissue's morphology for analysis at a later point in time. The following described procedures were performed on both tested samples and on residual thrombus material. Material cut adjacent to the tested sample was specifically tracked for comparative purposes during the histological analysis. Samples were fixated for 48-72 hours before being washed with PBS and processed in a histokinette. During processing, the samples are first dehydrated by placing the samples in increasing concentrations of alcohol (70-100%). Secondly, Xyleen is used to remove the alcohol and lastly the samples are placed in paraffin wax, allowing it to infiltrate the tissue. Following the tissue processing, samples are embedded in a block of paraffin wax.

Sectioning and staining

After processing, the paraffin block including the embedded sample, was sectioned on a microtome. Sectioning was done at a depth of 100 μm and 200 μm , measured from the first full contact section, cutting 8 sections at a time. The 5 μm sections are placed on a glass slide and incubated. The sections are then stained in order to visualize the individual components present in the tissue. A Haematoxylin-Eosin stain was used to visualise of individual erythrocytes, leukocytes and fibrin fibers and platelets combined. Erythrocytes are coloured light red, the nucleus of leukocytes turn dark purple and fibrin/platelets pink. Figure C.1 illustrates 2 samples, of which the components of interest are highlighted. Fibrin/platelet rich areas are marked by the triangle, red blood cell rich areas with the circle and leukocytes are appointed by the arrows.

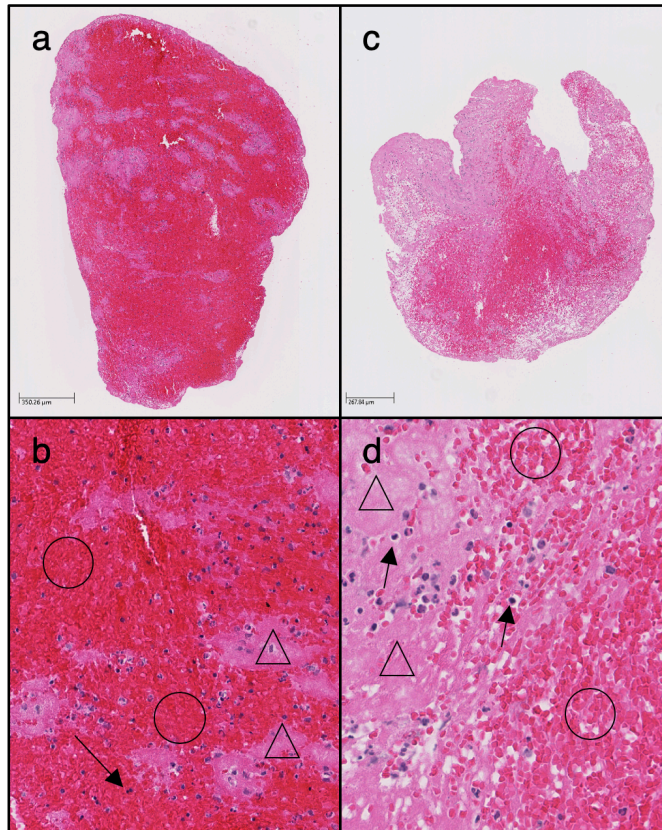


Figure C.1: Two samples: (a & b) represent a F/P moderate-low samples and (c & d) a F/P moderate-high sample. The components of interest are highlighted as followed: Fibrin/platelet rich areas are marked by the triangle, red blood cell rich areas with a circle and leukocytes are appointed by the arrows.

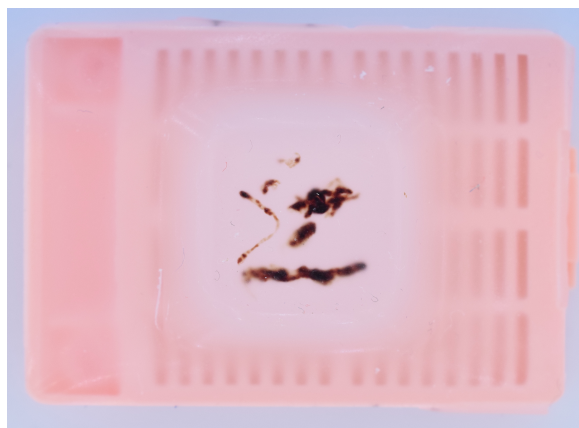


Figure C.2: Embedded thrombus material in paraffin wax.

Histological analysis

Sections were scanned with a nano-zoomer to create digital images. Both the tested samples and residual material (cut adjacent to the tested sample) were visual inspected and compared to assess the quality of the slides and the influence of the compression test on the samples composition. It was found that for a portion of the tested sample, the composition at a depth of 100 μm deviated slightly from that of the untested samples. This effect was only minimally present in the samples cut at a depth of 200, making those sections most suitable for histological analysis.

The composition of each tested sample was quantitatively determined by analysing the sections in Orbit Image Analysis (version 3.15, Idorsia Pharmaceuticals Ltd, Allschwil). By manually appointing the tissue's structures of interest (Fibrin/platelets, erythrocytes and leukocytes), the image analysis software is trained to recognize similar structures throughout the entire section. This allowed for the separation of the individual components, based on both colour and structure. The quantitative fraction of each component is determined with regards to the section total surface area. The analysis was performed independently by two observers in Orbit Imaging software.

C.2. Results

The results of the histological quantification of each thrombus samples can be found in table C.1. Two samples were excluded as they could not be quantified adequately according to the protocol used for quantification of the other samples. This was caused by the excessive amount of, presumably, cytoplasm which was present in the section. The cytoplasm stained similar as Fibrin/Platelets, and therefore overestimated the Fibrin/Platelet content. Although this observation is of interest for future analysis, it has led to the exclusion of the sample in this study by recommendation of an experienced histopathologist. This (excessive) presence of cytoplasm was not found in other samples. Detailed images of the excluded sample are presented in figure C.3

Table C.1: Histological composition of tested samples

	Observer 1			Observer 2			Averaged		
	RBC	F/P	Leuko	RBC	F/P	Leuko	RBC	F/P	Leuko
TBM01 P1 S2 a	3.6	95.4	1.0	3.5	96.0	0.5	3.5	95.7	0.8
TBM02 P1 S1 b	46.4	52.4	1.3	40.3	58.6	1.1	43.3	55.5	1.2
TBM03 P1 S1 b	27.3	70.3	2.4	15.1	83.3	1.6	21.2	76.8	2.0
TBM04 P2 S1 a	81.1	18.8	0.1	73.0	26.8	0.1	77.1	22.8	0.1
TBM04 P2 S3 a	85.0	14.3	0.7	85.6	13.3	1.1	85.3	13.8	0.9
TBM04 P4 S1 a	6.7	92.8	0.5	10.7	89.0	0.3	8.7	90.9	0.4
TBM04 P4 S2 a	11.3	88.2	0.5	14.4	85.1	0.5	12.9	86.7	0.5
TBM05 P1 S1 a	1.1	98.5	0.4	0.6	99.1	0.3	0.9	98.8	0.3
TBM05 P1 S1 b	2.0	97.8	0.2	4.8	94.9	0.4	3.4	96.3	0.3
TBM05 P1 S2 a	2.4	97.1	0.5	0.5	99.3	0.2	1.5	98.2	0.4
TBM05 P4 S1 a	0.4	99.6	0.1	0.4	99.5	0.1	0.4	99.5	0.1
TBM06 P1 S1 b	71.2	26.3	2.5	69.0	28.6	2.3	70.1	27.5	2.4
TBM07 P2 S1 b	5.8	85.9	8.4	10.3	86.9	2.8	8.1	86.4	5.6
TBM07 P2 S2 a	5.9	91.9	2.3	5.8	92.6	1.6	5.8	92.2	1.9
TBM08 P1 S1 a	25.7	72.8	1.5	20.7	78.4	0.9	23.2	75.6	1.2
TBM08 P1 S2 a	49.7	49.5	0.8	45.8	53.5	0.7	47.7	51.5	0.8
TBM08 P2 S1 a	24.6	74.2	1.2	23.3	74.8	2.0	23.9	74.5	1.6
TBM09 P1 S1 a	56.3	42.6	1.1	63.1	35.4	1.5	59.7	39.0	1.3
TBM09 P1 S1 b	60.0	38.5	1.4	66.0	33.2	0.8	63.0	35.9	1.1
TBM09 P3 S1 a	59.7	38.8	1.4	61.0	37.3	1.7	60.4	38.0	1.6
TBM09 P5 S1 a	32.3	66.5	1.2	31.7	66.8	1.5	32.0	66.6	1.4
TBM10 P2 S1 a	0.8	99.0	0.2	0.3	99.5	0.1	0.6	99.3	0.1
TBM10 P2 S2 a	0.3	99.6	0.2	0.1	99.7	0.1	0.2	99.7	0.1
TBM11 P1 S1 a	32.8	64.3	2.9	33.2	64.6	2.2	33.0	64.4	2.5
TBM11 P1 S2 a	41.2	58.0	0.8	41.1	57.4	1.5	41.1	57.7	1.1
TBM12 P1 S1 a	86.5	12.4	1.1	86.9	12.2	0.9	86.7	12.3	1.0
TBM12 P1 S1 b	88.6	10.7	0.6	88.6	10.8	0.6	88.6	10.8	0.6
TBM12 P1 S1 c	85.8	13.8	0.4	78.0	21.8	0.3	81.9	17.8	0.3
TBM12 P1 S2 a	96.0	2.9	1.0	86.1	12.9	1.0	91.1	7.9	1.0
TBM13 P1 S1 a	46.1	52.8	1.1	47.5	49.7	2.8	46.8	51.3	1.9
TBM13 P1 S2 a	62.4	35.9	1.7	65.1	33.8	1.1	63.7	34.8	1.4
TBM14 P1 S1 a	65.4	33.7	0.9	51.5	47.3	1.1	58.4	40.5	1.0
TBM14 P1 S1 b	38.7	60.4	0.8	42.0	57.3	0.6	40.4	58.9	0.7
TBM15 P1 S1 a	50.0	48.7	1.3	38.7	59.8	1.6	44.3	54.2	1.4
TBM17 P1 S1 a	47.6	51.3	1.1	33.5	65.3	1.3	40.5	58.3	1.2
TBM18 P2 S1 a	40.1	59.6	0.3	43.5	56.3	0.2	41.8	58.0	0.2
TBM19 P1 S1 a	1.3	98.5	0.2	4.1	95.5	0.5	2.7	97.0	0.3
TBM19 P1 S2 a	2.6	97.2	0.2	0.3	99.7	0.1	1.4	98.4	0.1
TBM20 P1 S1 a	6.3	91.6	2.1	7.2	90.8	2.0	6.8	91.2	2.1
TBM20 P1 S2 a	21.5	77.1	1.4	12.3	83.3	4.4	16.9	80.2	2.9
TBM20 P1 S2 b	35.7	62.7	1.6	16.0	82.6	1.3	25.9	72.7	1.5
TBM20 P1 S2 c	21.0	75.2	3.8	16.6	81.5	2.0	18.8	78.3	2.9
TBM21 P1S1 a	25.1	73.8	1.0	24.0	74.3	1.7	24.6	74.1	1.4
TBM21 P1S1 b	73.7	25.0	1.3	74.2	24.1	1.7	74.0	24.6	1.5

Histological composition of each sample. Analysis performed in Orbit by two observers. Averaged value between observers was taken as the final histological composition. RBC = Red blood cells, F/P = Fibrin and platelets, Leuko = Leukocytes. All values are given in percentages (%).

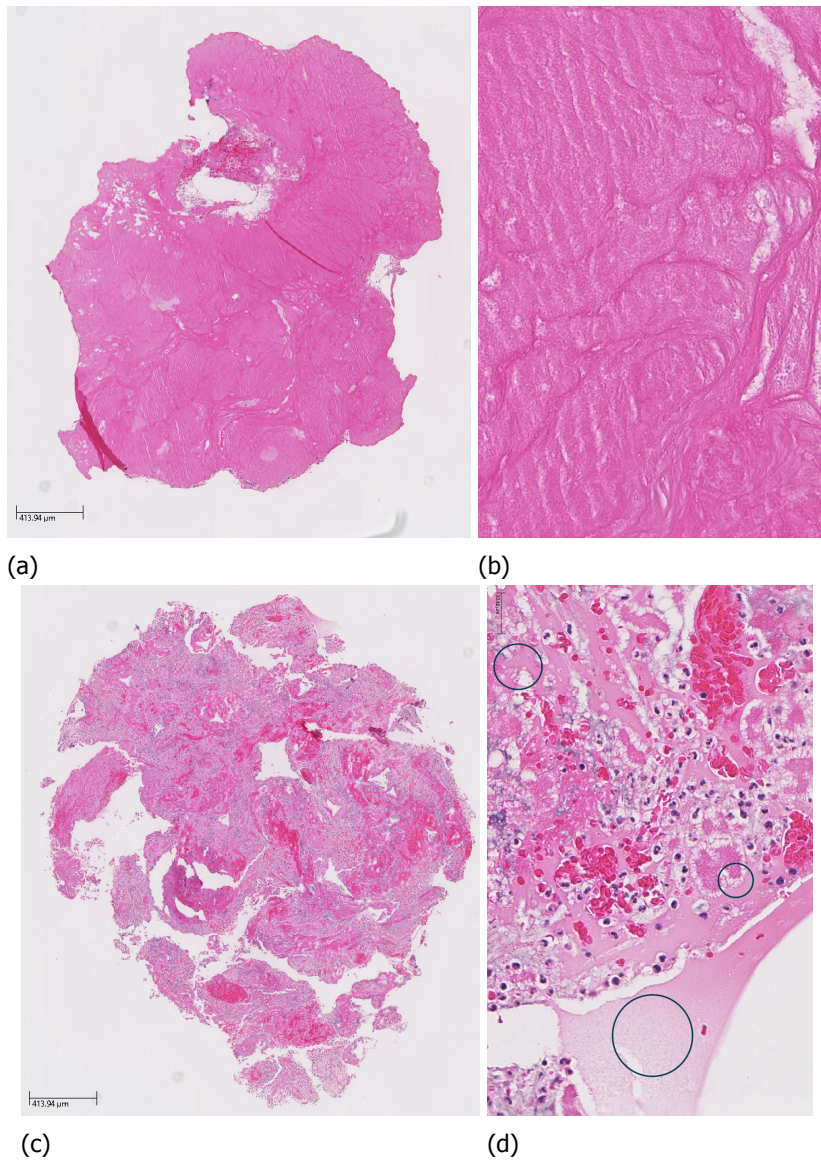


Figure C.3: **Histological images of (a & b) a fibrin/platelet rich sample and (c & d) a sample with excessive amounts of cytoplasm. It can be seen that the fibrin rich sample consist of only fibrin/platelet content in image b. In image d a few, but not all, cytoplasm rich areas are encircled. The cytoplasm is present throughout a large part of the sample, surrounding most of the additional red blood cell and leukocyte content.**

D

Constitutive modelling

D.1. Application of the Mooney-Rivlin model to experimental data

In order to obtain the mechanical properties of tested samples, first constitutive models were fitted to the experimentally gained test data. Fitting of the models was performed in Abaqus (2016, Dassault Systems, Johnston, Ri), with incompressibility and isotropy assumed for all samples. Multiple models were applied, with the first order Mooney-Rivlin model providing the most optimal fit over the entire range of samples.

For an incompressible material, the strain energy density function (W) is given as:

$$W = C_{10}(I_1 - 3) + C_{01}(I_2 - 3) \quad (\text{D.1})$$

Where I_1 and I_2 are the first and second strain invariants of the left Cauchy-Green deformation tensor, given as:

$$I_1 = \lambda_1^2 + \lambda_2^2 + \lambda_3^2 \quad (\text{D.2})$$

$$I_2 = \lambda_1^2\lambda_2^2 + \lambda_1^2\lambda_3^2 + \lambda_2^2\lambda_3^2 \quad (\text{D.3})$$

For a uni-axial compression test, where λ_1 is the stretch in the loading direction, the following holds:

$$\lambda_1 = \lambda, \quad \lambda_2 = \lambda_3 = \frac{1}{\sqrt{\lambda}} \quad (\text{D.4})$$

As is described in section D.2, the nominal stress is given by:

$$\sigma_{nominal} = \frac{\partial W}{\partial \lambda} = 2(1 - \lambda^{-3})(\lambda C_{10} + C_{01}) \quad (D.5)$$

Abaqus applies least squares minimization to determine the material constants C_{10} and C_{01} . As we are using a phenomenological model, these constants do not describe a physiological relation but are merely obtained in order to achieve the most optimal fit to the experimental data. Acquired material constants were used for further derivation of mechanical properties, performed in Matlab (R2016a, The Mathworks company).

To describe the non-linear mechanical behavior of these tested samples, both the secant and tangent moduli have been determined at multiple strains. The secant modulus is defined as the increase in stress over a range of strain (slope of a line intersecting both the origin and a point of interest on a stress-strain curve). The tangent modulus is defined as the slope of a line tangent to any point of interest on the curve, which can be determined by taking the first derivative of an equation describing the curve.

$$Secant E_{0-x} = \frac{\sigma_x}{\lambda_x - 1} \quad (D.6)$$

$$Tangent E_x = \frac{\partial \sigma}{\partial \lambda} = 2C_{10} + 4\lambda_x^{-3}C_{10} + 6\lambda_x^{-4}C_{01} \quad (D.7)$$

Where x denotes the percentage of compressive deformation at the point of interest on the stress-strain curve, λ_x the stretch ratio corresponding to x percentage of deformation and C_{10} and C_{01} are the material constants belonging to the Mooney-Rivlin model describing the sample behaviour. An elaborate derivation of the stress equation for a Mooney-Rivlin model is provided in the following section.

D.2. Derivation of the stress equation for a Mooney-Rivlin fit

For an incompressible and isotropic hyperelastic material, the Cauchy stress, expressed in principal stretches, is given by:

$$\sigma_a = -p + \lambda_a \frac{\partial W}{\partial \lambda_a} \quad (D.8)$$

Where σ_a is the Cauchy stress in the principal direction a , W the strain energy density function, λ the principal stretch in direction a and p the hydrostatic pressure. In case of a (incompressible and isotropic) Mooney-Rivlin material, the strain energy density function (W) is given by:

$$W = C_{10}(I_1 - 3) + C_{01}(I_2 - 3) \quad (D.9)$$

Substituting equation D.2 and D.3, the first invariant (I_1) and second invariant (I_2) of the left Cauchy-green tensor, in equation D.8 gives us the following strain energy density function:

$$W = C_{10}(\lambda_1^2 + \lambda_2^2 + \lambda_3^2 - 3) + C_{01}(\lambda_1^2\lambda_2^2 + \lambda_1^2\lambda_3^2 + \lambda_2^2\lambda_3^2 - 3) \quad (\text{D.10})$$

The Cauchy stress in the first, second and third principal direction is given by:

$$\sigma_1 = -p + \lambda_1 \frac{\partial W}{\partial \lambda_1} \quad (\text{D.11})$$

$$\sigma_2 = -p + \lambda_2 \frac{\partial W}{\partial \lambda_2} \quad (\text{D.12})$$

$$\sigma_3 = -p + \lambda_3 \frac{\partial W}{\partial \lambda_3} \quad (\text{D.13})$$

Differentiating D.10 with respect to λ_1 and λ_2 and substituting in D.11 and D.12 respectively gives:

$$\sigma_1 = -p + \lambda_1(2C_{10}\lambda_1 + C_{01}(2\lambda_1\lambda_2^2 + 2\lambda_1\lambda_3^2))$$

$$\sigma_1 = -p + 2\lambda_1^2(C_{10} + C_{01}(\lambda_2^2 + \lambda_3^2)) \quad (\text{D.14})$$

and

$$\sigma_2 = -p + \lambda_2(2C_{10}\lambda_2 + C_{01}(2\lambda_2\lambda_1^2 + 2\lambda_2\lambda_3^2))$$

$$\sigma_2 = -p + 2\lambda_2^2(C_{10} + C_{01}(\lambda_1^2 + \lambda_3^2)) \quad (\text{D.15})$$

For a uni-axial compression test, the sample is loaded only in one direction, therefore $\lambda_1 = \lambda$ and $\lambda_2 = \lambda_3 = \frac{1}{\sqrt{\lambda}}$. Applying this to equation D.14 and D.15 gives:

$$\sigma_1 = -p + 2\lambda^2(C_{10} + C_{01}(\frac{2}{\lambda})) \quad (\text{D.16})$$

$$\sigma_2 = -p + \frac{2}{\lambda}(C_{10} + C_{01}(\lambda^2 + \frac{1}{\lambda})) \quad (\text{D.17})$$

To find the hydrostatic pressure (p), we know that the principal stress in $\sigma_2 = \sigma_3 = 0$. Rewriting D.17 gives:

$$p = \frac{2}{\lambda}(C_{10} + C_{01}(\lambda^2 + \frac{1}{\lambda})) \quad (\text{D.18})$$

Substituting equation D.18 in equation D.16, we get:

$$\sigma_1 = -\frac{2}{\lambda}(C_{10} + C_{01}(\lambda^2 + \frac{1}{\lambda})) + 2\lambda^2(C_{10} + C_{01}(\frac{2}{\lambda}))$$

$$\sigma_1 = 2C_{10}(\frac{-1}{\lambda} + \lambda^2) + 2C_{01}(-\lambda - \frac{1}{\lambda^2} + 2\lambda)$$

$$\sigma_1 = 2C_{10}(\lambda - \frac{1}{\lambda^2}) - 2C_{01}(\frac{1}{\lambda^3} - 1) \quad (D.19)$$

To express the first Piola-Kirchoff stress (nominal stress) in terms of Cauchy stress, the following formula holds:

$$\sigma_{nominal} = \frac{\sigma_{cauchy}}{\lambda} \quad (D.20)$$

If we apply equation D.20 tot D.19, we get a Piola-Kirchoff (nominal) stress equation as:

$$\sigma_{nominal} = 2C_{10}(\lambda - \frac{1}{\lambda^2}) - 2C_{01}(\frac{1}{\lambda^3} - 1) \quad (D.21)$$

Which can be rewritten to the following:

$$\sigma_{nominal} = 2(\lambda C_{10} + C_{01} - \frac{C_{10}}{\lambda^2} - \frac{C_{01}}{\lambda^3})$$

$$\sigma_{nominal} = 2(1 - \frac{1}{\lambda^3})(\lambda C_{10} + C_{01}) \quad (D.22)$$

Where D.22 is our final nominal stress equation, used for the determination of the material constant C_{10} and C_{01} . The stretch ratio in the loading direction (λ) is found as followed:

$$\lambda = \epsilon + 1$$

Where, in case of the performed compression test, the applied strain (ϵ) is a negative value between 0 and -1 and the stretch ratio (λ) a value between 0 and 1.

D.3. Matlab code for calculation of secant and tangent moduli

```

1      %%%%%%%%%%%%%%%%%%%%%%%%%%%%%%%%%%%%%%%%%%%%%%%%%%%%%%%%%%%%%%%%%%%%%%%%%%%%
2      % This script imports the C10 and C01 constants derived by fitting the Mooney-
          Rivlin model to the experimental test data gathered by means of an
          unconfined compression test. The script uses the material constants to
          determine the secant and tangent modulus at multiple strains. The
          constants are imported from the "Modeling_data" excel file, in the "
          Constants" sheet.
3      %% %%%%%%%%%%%%%%%%%%%%%%%%%%%%%%%%%%%%%%%%%%%%%%%%%%%%%%%%%%%%%%%%%%%%%%%%%%%
4
5      close all
6      clear all
7      clc
8
9      C10 = xlsread('Modeling_data', 'Constants', 'C6:C48'); % Importing constant
          C10 from excel
10     C01 = xlsread('Modeling_data', 'Constants', 'D6:D48'); % Importing constant
          C01 from excel
11
12     % Stretch ratios in axial direction (1 - strain), 5% - 80%
13     SR = [0.95, 0.90, 0.80, 0.70, 0.60, 0.50, 0.40, 0.30, 0.25, 0.20];
14
15
16     % Calculating the secant moduli at the determined strain
17     % Stress equation = 2 * (1 - SR^(-3)) * (SR*C10 + C01); where SR =
          StretchRatio
18     % Secant modulus is determined by deviding the stress by the corresponding
          strain
19
20     SecMod = zeros(length(SR),length(C10)); %empty array of zeros to store secant
          moduli
21     k = 1;
22     for ii = 1:length(SR)
23         for j = 1:length(C10)
24
25             Stresseq = 2*(1-(SR(ii))^-3)*(SR(ii)*C10(j)+C01(j)); % stress equation
26             SecMod(k,j) = Stresseq/(1-SR(ii)); % stress/ strain
27
28         end
29         k=k+1;
30     end
31
32
33     % Calculating tangent modulus at the determined strain
34     % Derivative of stress equation = 2*C10 + 4*SR^(-3)*C10 + 6*SR^(-4) * C01
35     % Tangent modulus = output of derived stress equation at given strain
36
37     TanMod = zeros(length(SR),length(C10)); %empty array of zeros to store the
          tangent moduli
38     k = 1;
39     for ii = 1:length(SR)
40         for j = 1:length(C10)
41
42             dStresseq = 2*C10(j) + 4*SR(ii)^(-3)*C10(j) + 6*SR(ii)^(-4)*C01(j); %
          derivative of stress equation
43             TanMod(k,j) = dStresseq;
44
45         end
46         k=k+1;
47     end
48
49
50
51

```

```

52 %% Determining the moduli of Subgroups %%%%%%%%%%%
53 % This script derives the secant and tangent moduli of each subgroup. The
    derived material constants for each subgroup are imported from excel.
54 %%%%%%%%%%%
55
56 SUB_C10 = xlsread('Modeling_data', 'Constants', 'G6:G25'); % Importing
    constant C10 from excel for T1,T2,T3,T4
57 SUB_C01 = xlsread('Modeling_data', 'Constants', 'H6:H25'); % Importing
    constant C01 from excel for T1,T2,T3,T4
58
59 % Stretch ratios in axial direction (1 - strain), 5% - 80%
60 SUB_SR = [0.95, 0.90, 0.80, 0.70, 0.60, 0.50, 0.40, 0.30, 0.25, 0.20];
61
62 % Calculating the secant moduli at the determined strain
63 % Stress equation = 2 * (1 - SR^(-3)) * (SR*C10 + C01); where SR =
    StretchRatio
64 % Secant modulus is determined by deviding the stress by the corresponding
    strain
65
66 SUB_SecMod = zeros(length(SUB_SR),length(SUB_C10)); %empty array of zeros to
    store secant moduli
67 c = 1;
68 for vv = 1:length(SUB_SR)
69 for b = 1:length(SUB_C10)
70
71 SUB_Stresseq = 2*(1-(SUB_SR(vv))^(-3))*(SUB_SR(vv)*SUB_C10(b)+SUB_C01(b)); %
    stress equation
72 SUB_SecMod(c,b) = SUB_Stresseq/(1-SUB_SR(vv)); % stress/ strain
73
74 end
75 c=c+1;
76 end
77
78
79 % Calculating tangent modulus at the determined strain
80 % Derived stress equation = 2*C10 + 4*SR^(-3)*C10 + 6*SR^(-4) * C01
81 % Tangent modulus = output of derived stress equation at given strain
82
83 SUB_TanMod = zeros(length(SUB_SR),length(SUB_C10)); %empty array of zeros to
    store the tangent moduli
84 c = 1;
85 for vv = 1:length(SUB_SR)
86 for b = 1:length(SUB_C10)
87
88 SUB_dStresseq = 2*SUB_C10(b) + 4*SUB_SR(vv)^(-3)*SUB_C10(b) + 6*SUB_SR(vv)
    ^(-4)*SUB_C01(b); % derivative of stress equation
89 SUB_TanMod(c,b) = SUB_dStresseq;
90
91 end
92 c=c+1;
93 end

```

D.4. Results

In order to find the most optimal fit to the experimental data, the Neo-Hookean, Mooney-Rivlin, Oged, Yeoh and Arruda-Boyce models were fitted in Abaqus. Taking into account the entire range of samples, the Mooney-Rivlin model provided the best fit for to the experimental data.

Figure D.1 shows the fitted Mooney-Rivlin models to the averaged data of the 4 subgroups. The derived material constant are provided in table D.1. The constant provide the means for further modelling application to simulate the behaviour of typical thrombus types.

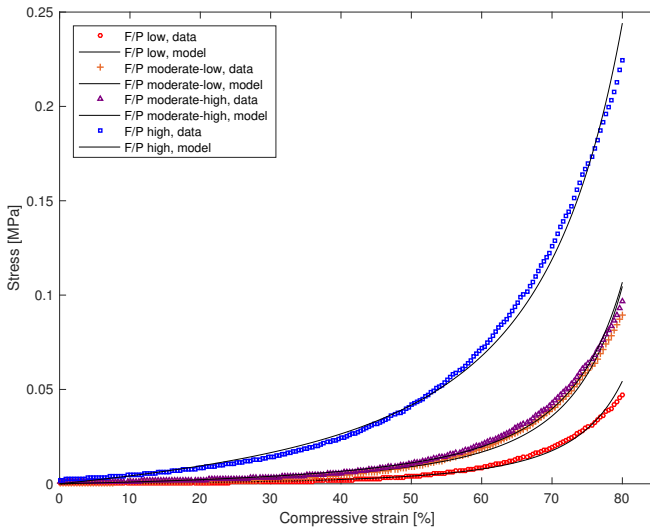
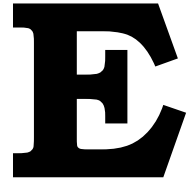


Figure D.1: **Averaged experimental data and fitted models of each subgroup. The coloured markers represent the experimental data, whilst the solid lines are the fitted models.**

Table D.1: Material constant for fitted Mooney-Rivlin

	C10	C01	NRMSE
F/P low	240.1	171.3	0.8897
F/P moderate-low	763.5	269.08	0.8891
F/P moderate-high	1201.0	190.6	0.9213
F/P high	6651.6	-345.9	0.9289

Material constants derived with the first order Mooney-Rivlin model. The models were fit to the initial loading curve of the averaged experimental data of each subgroup.



Micro indentation

To determine the mechanical properties at small strains and on a local scale, micro-indentation experiments were performed on a subset of the samples, prior to the unconfined compression test. As this experiment has not been included in the scientific paper, details are elaborated on in this appendix.

Micro-indentation is a technique that allows the user to determine the material properties of a sample by applying small strain deformations to the surface of the tissue, within the micro-meter range. Although both micro-indentation and compression tests rely on the deformation of a tissue, there are several differences between the techniques. The advantage of micro-indentation, is the ability to determine the properties by means of a non-destructive experiment. This provides several possibilities, such as performing the experiment at multiple time points or performing additional experiment subsequent to the indentation test. Secondly, the relatively small size of the micro-indenter tip allows for the testing of samples of a much smaller size, where the accuracy and sensitivity of most compression tester is not high enough. However, the drawback is that the properties are only determined in the low strain regime, as the maximum indentation depth should not exceed 10% of the samples height and for relatively larger samples (in the mm range) the maximum achievable indentation depth is often a lot lower. Furthermore, due to the sensitivity of the equipment, additional influential factors should be taken into account, including acoustic vibrations, irregularities in surface topography and adhesive forces between the sample and the indenter.

E.1. Methods

A commercial nano-indenter (Piuma, Optics 11, Amsterdam) was used to perform the micro-indentation experiments. To analyse the sample's stiffness, the indenter uses a probe that consist of an optical fiber, a cantilever and the indentation tip,

as is shown in figure E.1a. A laser signal travels through the optical fiber and is projected on to the cantilever, whilst the reflection from the cantilever is simultaneously detected by the optical fiber. As the probe moves vertically downwards, and the tip encounters a surface, cantilever bending will induce a shift in the refraction index, and therefore the measured signal, which is recorded by the indenter. This provides the means to determine the height of the tip relative to the base of the cantilever and therefore the indentation depth.

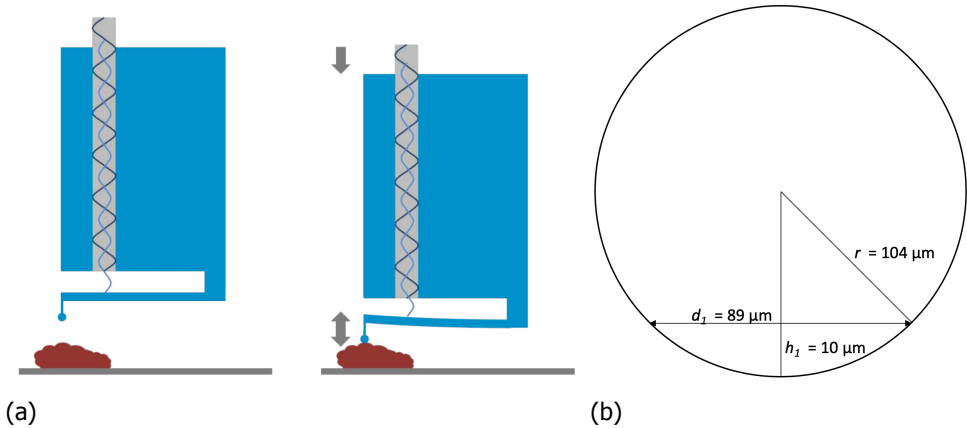


Figure E.1: **(a) A probe used by the micro-indenter. It consist of an optical fibre, cantilever and indenter tip. Contact with an object during downwards movement of the probe causes for bending of the cantilever. This results in a change in optical signal, which is used to determine the indentation depth. (b) Schematic drawing of indenter tip dimensions (not to scale). Where (r) is the radius of the indenter tip, h_1 the height from the bottom of the tip at an indentation of 10 micrometer and d the diameter of the tip at the height h_1 .**

For porous materials, such as bone or a fibrin network, the indenter tip diameter needs to be sufficiently large enough to eliminate the chance of it protruding through the pores, rather than compressing the samples surface. Based on scanning electron microscopy images of thrombus samples (found in literature), pore size was estimated to be no larger than 20-30 μm in diameter. A spherical tip with a radius of 104 μm and a cantilever stiffness of 0.49 N/m was chosen, as it can be calculated that at height of 10 μm measured from the bottom of the sphere (corresponding to the maximum indentation depth), the diameter of this tip is 89 μm (figure E.1b). This is sufficiently large enough to eliminate the possibility of the tip protruding through pores in the fibrous network. Further increasing the tip size strongly increases the risk of induced measurements noise, as the effect of acoustic vibrations are amplified by the relatively heavy tip. Under the right conditions it is possible to partially counteract these effect, however the facilities to achieve such an optimal environment were not present. Alternatively, the effect can be counteracted by increasing cantilever stiffness, however these probes are unsuitable for measuring soft thrombus material. Additionally, minimal movement of the sample is required to reduce measurement noise. Therefore, samples were adhered to a

Petri with use of 50% Polyethyleneimine solution (Sigma Aldrich, Darmstadt) and submerged in DMEM medium at room temperature. Polyethyleneimine is soluble and retains its adhesive properties only for a limited period of time, allowing for the sample to be removed without causing any damage to its structure.

The indentation profile consist of a 4x3 grid, a total of 12 indentations, with 200 μm spacing between indentation locations, in the horizontal plane. A flat top surface strongly improves the success rate of scan, as it reduces the chance of the probe making contact with the sample while moving between indentation locations. Additionally, an uneven surface can result in the contact between the sample and cantilever, rather than the tip, during indentation, which results in an erroneous measurement. In practice, the deformability of the soft biological tissue resulted in a significant number of incorrect measurements due to the above mentioned issues. In order to overcome these issues, two precautionary measures were taken. Firstly, if the top surface was not sufficiently parallel to the cantilever, the elevated side of the sample was placed away from the cantilever, and the lower end placed towards the cantilever (figure E.2a). Secondly, the initial indentation started at the elevated end of the sample, and moved towards the lower end of the samples (figure E.2b). This decreased the risk of the tip colliding with the sample during movement, and reduces the chance of an uneven topography resulting in unwanted contact with the cantilever.

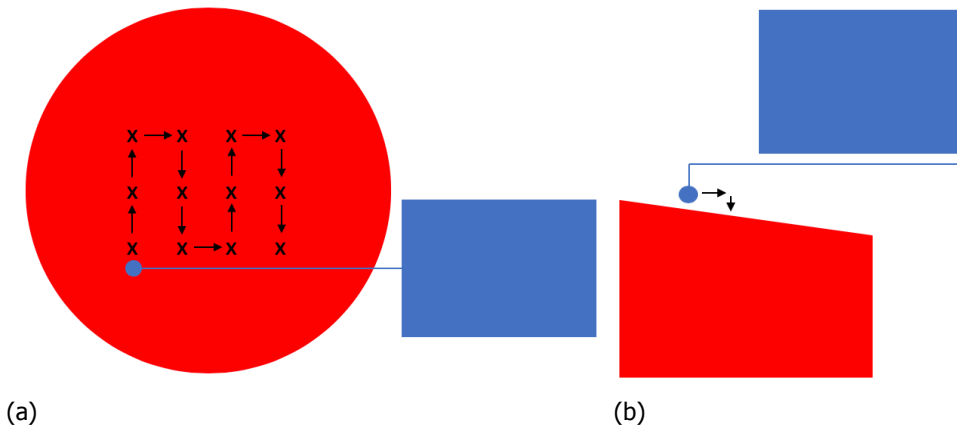


Figure E.2: **An illustration of the sample and indenter to exemplify the scanning grid, not made to scale. The sample is indicated in red, the indenter in blue, the indentation locations by the x and the direction of movement of the tip by the arrows. (a) A top view of sample and indenter, illustrating the 4x3 matrix. (b) A side view of the sample and indenter, illustrating the preferred direction of movement in order to minimize the risk of unwanted contact between the indenter and sample during movement and indentation.**

To align the tip at the correct height above the sample, the indenter automatically finds the surface by stepwise moving downwards until contact is made. Afterwards, it will raise by a defined height in order to start the experiment out of

contact. Adhesive forces can cause for the tip to stay in contact with the sample if the probe is not raised high enough. Therefore, the starting height of each indentation was preset at 10 μm above the sample's surface to ensure that the sample and tip were out of contact before the start of the experiment. This is required for accurate measurement and to determine the sample's stiffness by means of a fitted Hertzian model. In displacement-controlled mode, vertical cantilever displacement was set at 20 μm , allowing for a maximal sample indentation of 10 μm . Indentation and retraction speed were set at 10 $\mu\text{m/s}$ with a 1 second hold period between both phases. The Effective Young's modulus was determined with use of the Hertzian contact model, fit to 100% of the test data's loading curve, described as:

$$E_{eff} = 3P / (4R^{\frac{1}{2}} h^{\frac{3}{2}}) \quad (\text{E.1})$$

Where P is the applied load, R the radius of the spherical indenter tip, h the penetration depth and E_{eff} represents the effective composite elastic modulus. Of the 12 indentations performed on each sample, those that did not start out of contact were discarded as they were unsuitable for fitting of the Hertzian model. The E_{eff} of the remaining successful indentations were averaged to determine the final E_{eff} of each sample.

It must be noted that the Hertz model can be used with the assumption of certain conditions, including frictionless contact between bodies, elastic behaviour of a samples and homogeneity within the sample. Soft biological tissue usually is not homogeneous nor does it behave elastic. In an absolute elastic material, the energy transferred from the tip to the sample would be directly given back. However, as biological material is often viscoelastic, energy will dissipate as the stress is dispersed throughout the cells and fluid within the sample. This phenomenon is time-dependant and a higher indentation rate will lead to a larger resistance of the sample, resulting in a higher measured stiffness. To partially counteract this issue, one should find an optimal indentation rate where the effect is minimal. Heterogeneity can influence the measurement as the sample's structure might vary over the course of the indentation depth, altering the stiffness.

E.2. Results

Micro-indentation was performed on 12 samples prior to the unconfined compression test. Each indentation yields a Load-displacement curve, as is shown in figure E.3, where the indentation depth is represented on the x-axis and the applied load on the y-axis. It can be seen that the experiment starts out of contact, as during the first 10 μm displacement there is no increase in load. After contact is made, the load increases as a result of the indentation, with the sample exhibiting a near linear response. A decrease in the load is seen during the 1 second holding period, illustrating the materials viscoelastic behaviour. Lastly, hysteresis is observed during the unloading cycle and adhesive force cause for a negative load as the indenter tip pulls away from the sample.

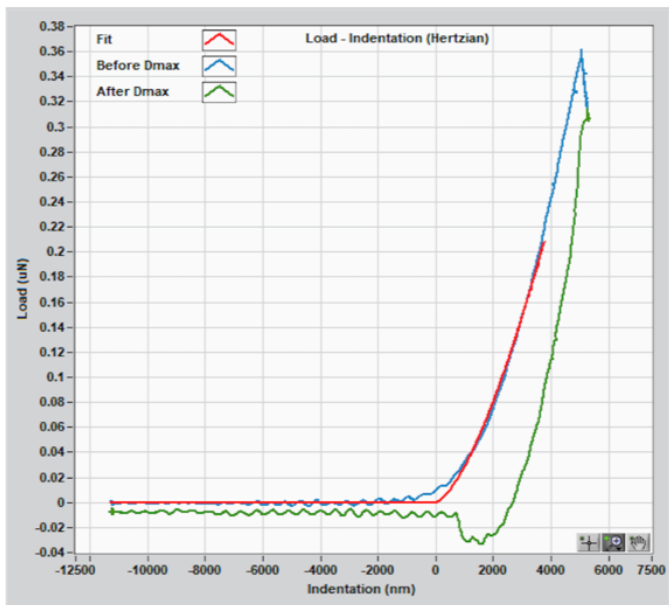


Figure E.3: **A typical load-displacement curve yielded from an indentation test. The blue line represent the loading/indentation phase, the green line the unloading/retraction phase and the red line the fitted Hertz model.**

On average, for each individual sample, 7/12 indentations were successful and could be used to determine the averaged E_{eff} . Two main causes accounted for failed indentations, both induced by the irregularities in the sample surface topography: 1) contact was made between the tip and sample before initiation of the indentation; 2) contact was made between the cantilever and sample, inducing measurement noise.

In figure E.4, the bars represent the composition of the tested samples and the corresponding E_{eff} , as an average of the successful indentations, is indicated by the marker. A (weak) positive correlation can be observed between fibrin & platelet content and the effective Young's modulus ($R=0.52$, $p=0.08$). Complementary to the compression test discussed in the scientific paper, this provides additionally evidence that sample composition has an effect on the stiffness.

It should be mentioned that this is only a subset of the samples tested with the compression tester and that a relatively large variance within the compression test data has been observed, especially looking at the fibrin & platelet rich samples. Based on the data gathered from the compression test, it can be suggested that for this analysis a bias has been introduced, causing for an underestimation of the correlation between fibrin & platelet content and stiffness. Observing samples 7-12 of the indentation test, which have a relatively high fibrin & platelet content (>70%), it can be seen from the results of the compression test that the stiffness of sample 7-11 is relatively low compared to the other samples with a comparable

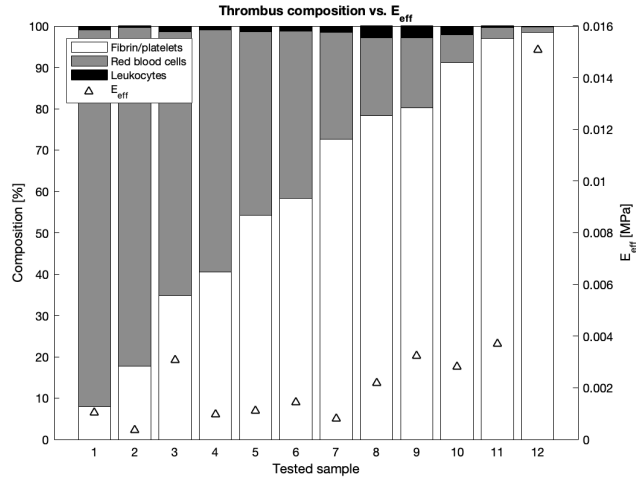


Figure E.4: **The bar chart represents the histological composition of the 12 samples tested by means of micro-indentation. The triangular markers indicate the Effective Young's modulus of each sample.**

fibrin & platelet content. Sample 12 on the other hand, is found to be relatively stiff compared to the other fibrin & platelet rich samples in the compression test, which is also reflected in the high E_{eff} measured with the indentation test. In other words, 5/6 samples used in the indentation experiment which have a relatively high fibrin & platelet content (>70%) are relatively soft compared to the other fibrin & platelet rich samples tested with the compression test. Bearing this in mind, it can be therefore be suggested that the correlation would have been stronger if the other samples, including the stiffer fibrin & platelet rich samples, would have been included in the analysis. In Table E.1, for each sample tested by means of indentation, the corresponding sample number of the compression test results (figure 4 in the scientific paper)

The results found by means of indentation have also been compared to the results found with the compression test. Under the assumption of a uniform strain distribution throughout the sample, the maximum indentation depth of 10 μm corresponds to approximately 1% strain of the entire sample's initial height. Therefore, the E_{eff} determined by micro-indentation was compared to the secant $E_{0-1\%}$ and tangent $E_{1\%}$ derived from the unconfined compression test. Only the tangent $E_{1\%}$ has been included in the graph, as values were very similar to those of the secant $E_{0-1\%}$. The results are represented in figure E.5. It is worth noting that, although currently assumed, the distribution of the strain will most likely not be uniform throughout the entire sample due to its viscoelastic nature. As a results, local deformation of tissue will be larger near the point of contact and will decrease with increasing distance from the point of contact. Therefore, the stress required to

Table E.1: Conversion table from indentation to compression test.

	Indentation test	Compression test
	1	1
	2	5
	3	9
	4	13
	5	16
Sample number	6	20
	7	24
	8	27
	9	28
	10	31
	11	34
	12	35

A conversion table which shows the the sample number used in figure 4 of the scientific paper, the results of the compression test, which corresponds to the sample number presented in figure E.4, the results of the indentation test.

achieve a certain indentation depth in a sample with non-uniform distribution will be higher compared to a sample where strain is distributed uniformly. Consequently, it would theoretically be more accurate to compare the E_{eff} determined at $10\mu\text{m}$ (by means of indentation) with a tangent E (determined by means of compression) corresponding to a strain that is larger than 1%. However, as we do not know the extent of the material's viscoelastic behaviour (which is also dependant on indentation speed), the non-uniform distribution of stress has not been taken into account.

From figure E.5 it can be seen that for these 12 samples, there is a positive correlation between fibrin & platelet content and the tangent $E_{1\%}$ ($R=0.61$, $p=0.037$). Furthermore, it can be seen the the effective Young's modulus follows the same trend as the Tangent $E_{1\%}$, although the difference in amplitude between the two measures becomes larger as fibrin & platelet content increases.

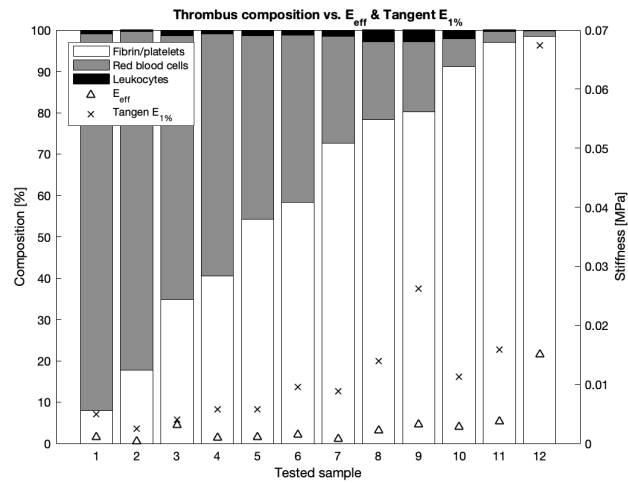


Figure E.5: **The bar chart represents the histological composition of the 12 samples tested by means of micro-indentation. The triangular markers indicate the Effective Young's modulus of each sample and the crosses represent the Tangent $E_{1\%}$ derived from the compression test results.**

F

Protocols

1.0 | Collection, Unconfined Compression & Fixation

Erasmus MC, 30.07.2019, Philip & Nikki

Materials

- TBM cart with pre-prepared equipment (instructions on preparation in protocol 0.0). Contents:
 - o Compression tester
 - o Compression tester laptop + charger
 - o Digital camera + light box + platform of 6.5cm high
 - o PBS solution
 - o Grid mat
 - o Box with utensils (3x small tweezers, 2x large tweezers, micro-scissors, ruler)
 - o Trimming fixture
 - o Set of microtome blades
 - o White, plastic box of 6.5cm high
 - o White tissue cassettes
 - o Pink tissue cassettes + foam for in cassettes.
 - o 2x pen, 2x pencil, pencil sharpener
 - o Non-absorbent paper
 - o 2x plastic trash bags
 - o Lab journal
 - o Plastic box
- Container (120 ml) with formalin (37% formaldehyde)
- Container (120 ml) with SEM-fixative (4% glutaraldehyde + 0.2M phosphate buffer)
- DMEM solution
- Small utensils (from lab Bram): 5x small plastic water basins, 1x glass beaker, 1x plastic pipette





The experiments are conducted at Ee-585.

Methods

0. Material collection

- 0.1. Thrombus material retrieved from acute ischemic stroke patients during thrombectomy is collected by the interventional radiology personnel in tissue containers with transparent DMEM (Figure 1).
- 0.2. Material is collected per-pass.
- 0.3. The material is collected by the researchers as soon as possible:
 - **Operating hours:** 08:30-21:00 – collection directly after thrombectomy
 - **Off hours:** 21:00-08:30 – collection the following morning at 08:30

1. Equipment setup

- 1.1. Turn on all equipment: power strip, compression tester laptop, light box
- 1.1. Start MEXE02 software. Via file>open, load “2mm sample” program and load the program in the actuator by pressing the “Data writing” button .
- 1.2. Start Labview software, load “Thrombus compression IO” (Documents > 1.Thrombus Bio-mechanics > 2. LabVIEW > Thrombus compression IO).
- 0.3 Turn on temperature regulator of the compression tester bath and set at 40°C (medium at 37±1.5 °C).
- 0.4 In LabVIEW:
 - 0.4.1 Open the block diagram (Ctrl+E), double click the “Write to measurement file” icon  and assign the correct folder and filename (folder: study ID; example ‘TBM05’ for study ID TBM05. File name: see Figure 2 about sample code) to save the test results.
 - 0.4.2 Set the interval to 40ms.
 - 0.4.3 Press the “run” button  for a live readout of the load cell.
 - 0.4.4 Press “tare load cell” button for 2 seconds.
- 0.5 In MEXE02:
 - 0.5.1 Open the manual control interface . Tick the “Start the teaching remote operation” box. If prompted, choose “writing all data (PC--> product)”.
 - 0.5.2 Lower the compression plate (using the manual control interface) until it is in contact with the base (readout of signal in LabVIEW) (*caution is taken to lower the plate with small steps to avoid damaging the load cell on impact!*) (tip: take steps of 1 mm, followed by 0.5 and 0.1 mm)
 - 0.5.3 When in contact, the plate is raised with 0.01mm, so it is no longer in contact with the base.
 - 0.5.4 Press “position preset” (this sets current position as home position).
 - 0.5.5 Press “CPOS+1” (this sets the positive limit at +0.01 mm).

1 Lab preparation

- 1.3.1 Place in fumehood: Formalin, SEM-fixative, glass beaker filled with PBS, large tweezers, plastic waste bag and tissues.
- 1.3.2 Place on working table: light box, camera, plastic platform, grid mat, utensils, trimming fixture, microtome blades, tissue cassettes, pens, pencils, PBS solution, non-absorbent paper, 5x small plastic water-basins, 1x plastic pipette, plastic waste bag, lab journal, tissues and gloves.
- 1.3.3 Prepare the non-absorbent paper in pieces of approximately 3x5 cm.

2. After receiving the material

- 2.1. Fill pre-heated compression tester bath with DMEM to the rim.
- 2.2. Register in lab journal:
 - 2.2.1. Time of start experiment.
 - 2.2.2. If any material is visibly present per pass container.

The following steps are performed for each pass.

3. Overview photo

- 3.1. Place non-absorbent paper with label (TBMwPx) on bottom and a ruler on top on the photography platform
- 3.2. Carefully remove all thrombus fragments of the first pass onto the photography level, including any stent-retriever if applicable.
- 3.3. Take the overview photo. Make sure the ruler and labeling are visible in the photo (Figure 3).

4. Removal of stent-retriever (if applicable)

- 4.1. The stent is cut open using micro-scissors and the thrombus is carefully removed using tweezers.

5. Overview photo without stent-retriever

- 5.1. Repeat photograph for all fragments of TBMwPx, now without stent.

6. Sample preparation

- 6.1. The thrombus is placed in the trimming fixture (Figure 4), such that the target area is aligned with the desired cutting length. *The researcher determines the target area and cutting length based on own consideration of what is possible for compression testing. Note: the cutting length will be the height of the sample during compression testing (Figure 5). Possible cutting lengths are: 1 mm / 2 mm / 3 mm.*
- 6.2. The thrombus is cut on both ends with the microtome blade making a smooth cutting motion.

7. Sample photo

- 7.1. Edit the label to TBMwPxSyz
- 7.2. Carefully place the sample on the photography level using small tweezers, such that one of the cutting surfaces faces upward, and take the photo (Figure 6).

8. Global compression prep

Figure 7-9 show the compression tester setup.

- 8.1. Important: if the sample was cut to 1 or 3 mm height, load the corresponding compression program ("*1mm sample*" or "*3mm sample*") in MEXE02. The home and limit positions do not need to be reset.
- 8.2. In MEXE02: Close the manual control interface.
- 8.3. In LabVIEW, press "*Raise to high position*".
- 8.4. Carefully place the sample on the testing platform in the pre-heated bath using small tweezers, such that the cutting surface that faced upward during photography, is facing upward (Figure 6).
- 8.5. In LabVIEW, press "*Set to starting height*" to lower the plate to the starting position. The compression plate can now warm up.

9. Sample preparation for SEM

- 9.1. The smallest sample that was adjacent to sample TBMwPxSyz is put into the white tissue cassette
- 9.2. Label white tissue cassette using pencil
- 9.3. Rinse the sample with a drop of PBS
- 9.4. Close the cassette
- 9.5. Rinse the cassette thoroughly in the beaker with PBS, then drop in glutaraldehyde.

10. Compression testing experiment

- 10.1. In LabVIEW:
 - 10.1.1. Press "Tare load cell" button for 2 seconds.
 - 10.1.2. Press "Start test & recording" button (the load cell readout will now be recorded in a TDMS file) (Figure 10 shows the compression profile).
 - 10.1.3. When the test has finished (when the compression plate has raised out of the medium), push the "Stop test" button to stop the recording.

11. Sample fixation

- 11.1. Label the pink tissue cassette for the tested sample using pencil and put a piece of foam in.
- 11.2. Carefully transfer the sample from the base to the pink tissue cassette using small tweezers, placing it in the same orientation as it was in the test, so the part facing upward during compression testing, is facing upward in the tissue cassette (Figure 11). Cover it with a second piece of foam. *NB: If the sample sticks to the compression plate: A small sheet of filtration paper or foam is lightly wetted with DMEM. Using tweezers, the sheet is moved in a straight upwards motion towards the compression plate, making contact with the sample. The sample can now be transferred from the paper to the cassette or placed in the cassette altogether.*
- 11.3. The cassette is thoroughly rinsed in PBS, then placed in formalin.

12. Testing remaining material from that pass

- 12.1. Step 7-12 are repeated for all other testable material of thrombus in the pass.

13. Fixation of restmaterial

- 13.1. Transfer the remaining material into a pink tissue cassette containing the label "TBMwPxrest"

14. Register in labjournal:

- 14.1. Study-ID
- 14.2. Name of researcher
- 14.3. Date
- 14.4. Time of start experiment
- 14.5. Any clinical information received from interventionalist and/or laborants
- 14.6. Per pass container: material present yes/no
- 14.7. Per tested sample:
 - 14.7.1. If surface area was smooth
 - 14.7.2. Placement on compression base
 - 14.7.3. If needed: schematic drawing (from the side) of tested sample while placed on the compression base

Leave tissue fixated for 24-28 hours.

Disposal of materials

- Biomaterial: all biomaterial (gloves, tissues, empty pass-containers with DMEM): in blue+yellow biomaterial container.
- Glutaraldehyde and formaldehyde in case of spill: in glutaraldehyde and formaldehyde container.
- Tissues/paper containing glutaraldehyde or formaldehyde: evaporate, then in blue+yellow biomaterial container.
- Cleaning of utensils used to handle thrombus: in sink, soap > dry > alcohol.

Figures

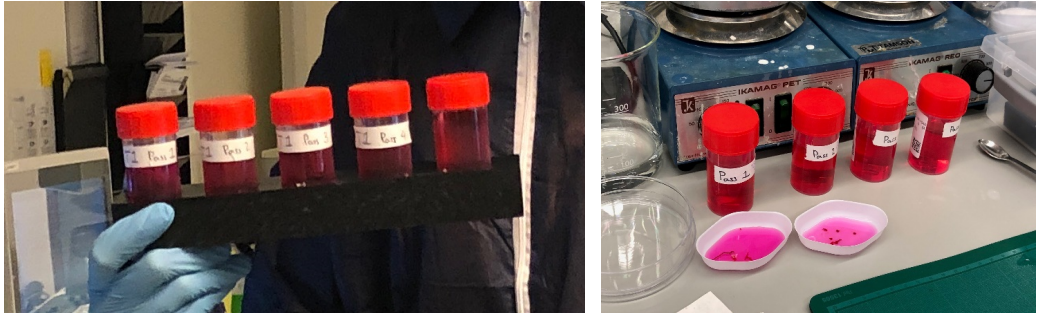


Figure 1: Per-pass collection of thrombi in DMEM-containers. Note: DMEM on these pictures is red transparent; during the experiments the DMEM color was changed to white transparent.

Figure 2: Thrombus sample code

“TBMwPxSyZ” is the thrombus sample code, where:

“w” = a number, identifying the unique TBM study ID

“x” = a number, identifying the pass in which the thrombus was retrieved

“y” = a number, identifying an individual thrombus belonging to pass “x”

“z” = a letter, identifying an individual sample belonging to thrombus “y”

Example - TBM01P2S2b:

TBM01 = study ID

P2 = 2nd pass

S2 = 2nd thrombus of that pass

b = 2nd sample that was biomechanically tested (or in case of a sample for SEM: that was directly adjacent to the biomechanically tested sample) from that thrombus.

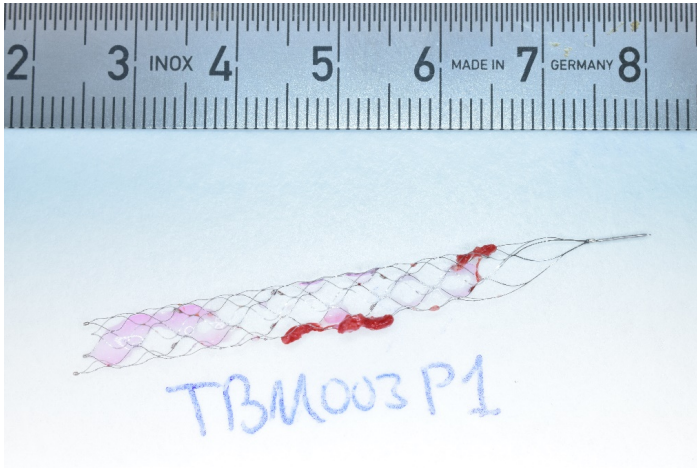


Figure 3: Example of overview photo of the first pass of a study subject. The material is photographed in the stent-retriever, if one is present.

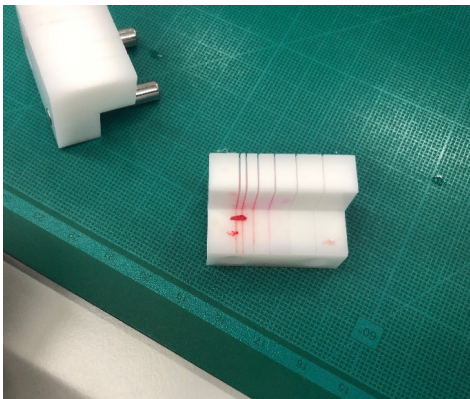


Figure 4: Trimming fixture.

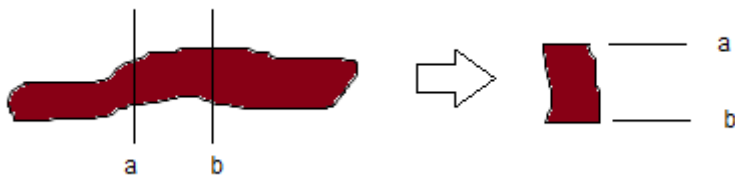


Figure 5: Schematic drawing of thrombus cutting for global compression. Left picture: The thrombus is cut in spot a and b. The part between a and b forms the sample. The orientation for global compression is shown on the right: the sample is turned 90 degrees clockwise or anticlockwise. This example shows a clockwise turn.

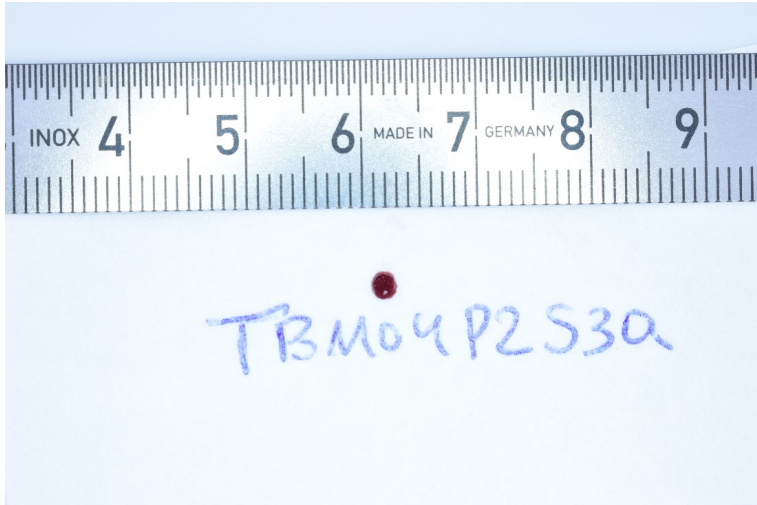


Figure 6: Example of a sample photo (indicates the first test sample of sample 3 of pass 2). The surfaces facing up- and downward are flat. This picture will be used to determine surface area of the part facing upward.

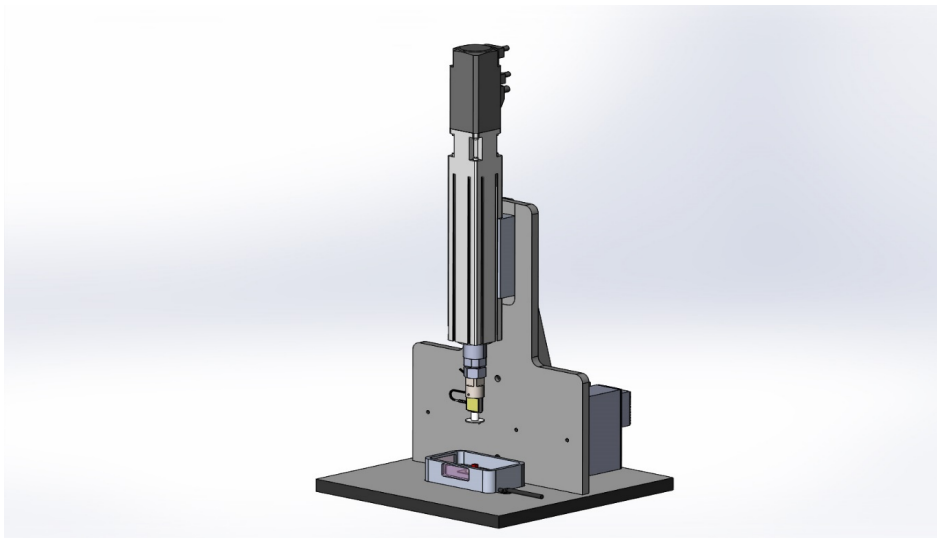


Figure 7: Schematic drawing of the unconfined compression tester.

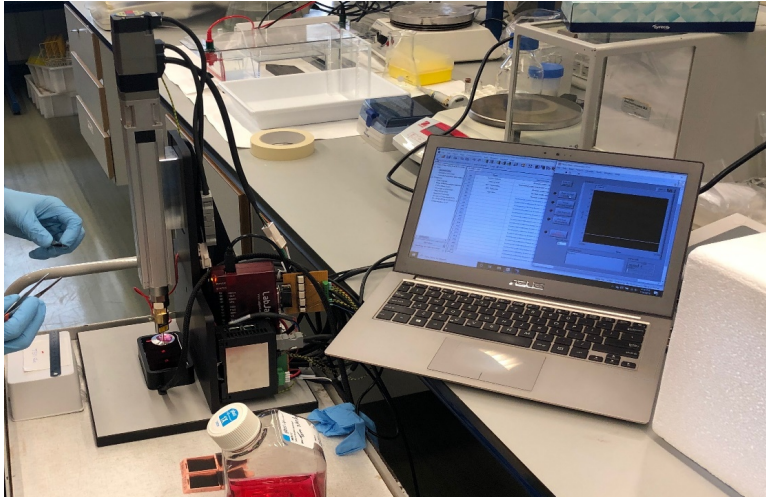


Figure 8: Compression testing setup. The compression tester (on the left) operates through the LabVIEW and MEXE02 software.

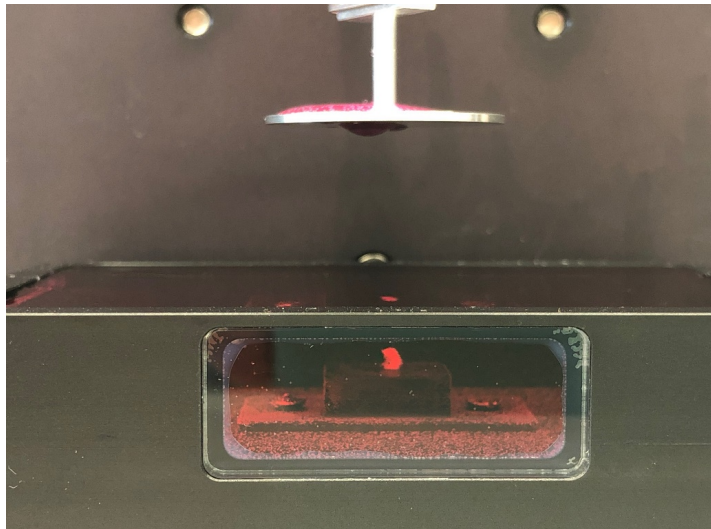


Figure 9: Close-up photo of cut thrombus sample before compression testing. The part of the sample that was facing upward in the sample photo, is facing upward.

Figure 10: Compression profile

- **Test type:** Cyclic compression test
- **Max strain ϵ_{\max} :** 80%
- **Strain rate:** 1 second per 10% strain -> 8 seconds to max strain
- **Hold:** hold at ϵ_{\max} is set at 0 seconds
- **Return rate:** 1 second per 10% strain -> 8 seconds to initial position
- **Repeat:** 20 cycles



Figure 11: The sample is placed in the pink tissue cassette, with the part that was facing upward during compression testing, facing upward in the cassette (as indicated).

2.0 | Tissue embedding

Erasmus MC, 09.08.2019, Philip & Nikki

Tissue processing: dehydration, clearing and infiltration

The tissue processor automates dehydration, clearing and infiltration of paraffin wax.

1. **Dehydration:** specimen immersed in ascending grades of alcohol to remove water and formalin.
2. **Clearing:** organic solvent e.g. xylene removes alcohol to allow infiltration with paraffin wax
3. **Infiltration:** specimen is infused with molten paraffin wax

Steps

- Wearing gloves, place tissue cassettes in tissue processor.
- Processor takes several hours to overnight.
- Wearing gloves, remove tissue cassettes from tissue processor.

Tissue embedding

Materials

- Paraffine Tissue Embedding Machine
- 1x small forceps (warmed)
- 1x big forceps
- Various size molds
- Tissue cassettes with the tissue

Preparation

Make sure the machine is turned on at least 1.5 hours before starting the embedding process.

Methods

- Place the tissue cassettes in the tissue container, in order.
- Open one cassette at a time, removing the top.
- Carefully remove upper the foam layer.
- Fill the mold with a shallow layer of paraffin
- Place the thrombus in the mold:
 - o For samples: with the part that was facing upward in the cassette, now facing downward. Tip: roll the sample over.
 - o For restmaterial (indicated with 'rest' on the tissue cassette): simply place it, such that the largest trans-sectional area will be available for histology.
- Allow the hot paraffin to cool down on the cool plate, only long enough to anker the tissue in place.
- Place your cassette top over the mold
- Completely fill with paraffin.
- Set the combined mold and cassette on the cold plate, neatly and in order. Immediate and rapid solidification of the paraffin block is desired in order to facilitate sectioning and to prevent the tendency to form large crystals in the wax.
- When the paraffin is sufficiently solidified (ca. 20 min), remove the block from the mold.
- Clean the block of excess paraffin without compromising the patient information on the block.
- Place in order in a box.

Cleaning/disposal of the materials:

1. Remove paraffin.
2. Clean pincet & molds:
 - a. Paraclear (in fumehood) + acetone afterwards (in fumehood).
 - b. Alternative: in stove (place paper tissue under it).

Figures

